Structural Optimization of Joined-Wing Beam Model with Bend-Twist Coupling Using Equivalent Static Loads

THESIS

Nicholas S. Green, Lieutenant Commander, USN

AFIT/GAE/ENY/09-J01

DEPARTMENT OF THE AIR FORCE
AIR UNIVERSITY

AIR FORCE INSTITUTE OF TECHNOLOGY

Wright-Patterson Air Force Base, Ohio

APPROVED FOR PUBLIC RELEASE; DISTRIBUTION UNLIMITED.

The views expressed in this thesis are those of the author and do not reflect the official policy or position of the United States Air Force, Department of Defense, or the United States Government.

AFIT/GAE/ENY/09-J01

Structural Optimization of Joined-Wing Beam Model with Bend-Twist Coupling Using Equivalent Static Loads

THESIS

Presented to the Faculty

Department of Aeronautical Engineering

Graduate School of Engineering and Management

Air Force Institute of Technology

Air University

Air Education and Training Command

In Partial Fulfillment of the Requirements for the

Degree of Master of Science in Aeronautical Engineering

Nicholas S. Green, BS

Lieutenant Commander, USN

June 2009

APPROVED FOR PUBLIC RELEASE; DISTRIBUTION UNLIMITED.

AFIT/GAE/ENY/09-J01

Structural Optimization of Joined-Wing Beam Model with Bend-Twist Coupling Using Equivalent Static Loads

Nicholas S. Green, BS
Lieutenant Commander, USN

Approved:

Robert A. Canfield (Chairman) — Date: 29 May 09

Eric D. Swenson (Member) — Date: 29 May 09

Donald Kunz (Member) — Date: 29 May 2009

Abstract

This study is based on the merger of two separate theories to further the efficiency with which joined-wing structural models are designed. The first theory is Geometrically Exact Beam Theory (GEBT). GEBT is a small strain beam theory which is capable of accurately capturing the geometric bend-twist coupling in beam elements that are experiencing large global deformations. This is crucial to the joined-wing problem as it is geometrically nonlinear. The second theory concerns Equivalent Static Loads (ESL). These ESL consist of a load vector that produces the same nodal displacements and rotations as those computed from a pure nonlinear analysis. The ESL displacements and rotations are then used to calculate ESL stresses. By merging these two theories into a single structural optimization effort, computational cost is reduced by orders of magnitude when compared to purely nonlinear response optimization efforts. It is shown that the final design obtained by the optimization is the same for both types of analysis. The final result is a much simpler model than a detailed finite element model of the joined-wing aircraft that can be optimized without significant loss in fidelity in a fraction of the time required for a single nonlinear response optimization cycle using finite element analysis.

Acknowledgements

I'd like to thank my wife. She rocks.

Nicholas S. Green

Table of Contents

List of Figures

List of Tables

Structural Optimization of Joined-Wing Beam Model with Bend-Twist Coupling Using Equivalent Static Loads

I. Problem Statement

The joined-wing configuration presented by Wolkovich in his 1986 paper has attracted much interest due to the advantages presented by such a configuration. Chief among these advantages are an increase in stiffness when compared to a classic wing and tail arrangement for a given weight when designed correctly [3]. Optimization efforts on joined-wing aircraft have steadily increased in complexity from fully stressed design [4] to efforts that incorporate the linear [5] and nonlinear [6] dynamic response using equivalent static loads. All of the aforementioned work has been done using finite element analysis as, until recently, beam theory was unable to fully capture the nonlinear geometric bend-twist coupling observed in the joined wing [7–10].

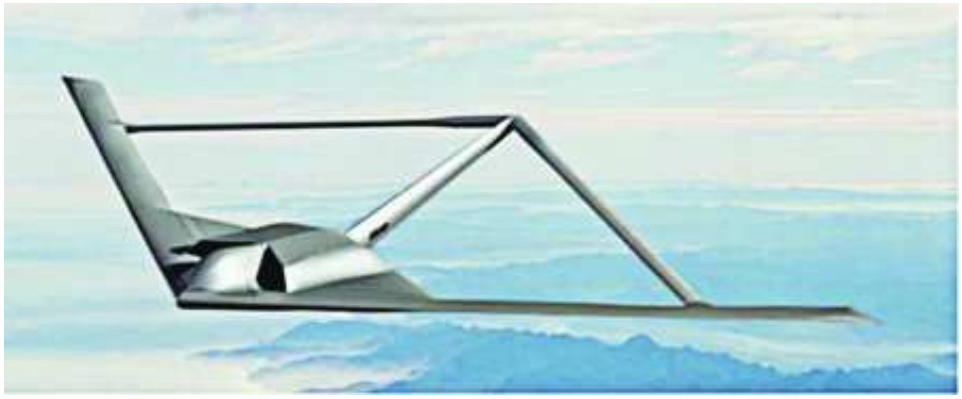

Figure 1.1: Boeing Sensorcraft design as proposed to Air Force Research Laboratory (AFRL)

The motivation for this research effort stems directly from the immense computational effort required to solve nonlinear problems with thousands of degrees of freedom. An example of a complex joined-wing model that to date has only been analyzed using finite element analysis is the Boeing Sensorcraft, shown in Fig. 1.1. This design has

been proposed to the Air Force Research Laboratory (AFRL) as a possible solution to a high altitude, long range, long endurance surveillance platform which will leverage the unique geometry of the joined-wing design in the deployment of its sensor arrays. Such a complex design would almost certainly benefit from an optimization effort which could include sizing of the wing box dimensions, the angles in both planform and head on views of the joined-wing, aerodynamic loads, and sensor effectiveness based on displacement of the wing from a nominal configuration in flight. Based on the cost of a single static nonlinear analysis on a model of the Boeing design, it is clear that an optimization that considers all of these design variables in a nonlinear response optimization would be unwieldy at best and intractable at worst. In an effort to reduce this computational overhead, this research explores the use of nonlinear structural analysis on a beam model of the joined-wing in a linear optimization routine using equivalent static loads in lieu of the nonlinear static response due to tip loads.

Early studies on the joined-wing show that bending due to a vertical tip load (with respect to the longitudinal axis of the vehicle) does not occur in the plane normal to the wing chord, but rather in the direction perpendicular to the plane created by the axes of the fore and aft wings [3]. This out-of-plane bending is then coupled with a twisting of the wing structure due to the geometry of the wings.

Simpler, classic wing box designs were often modeled as an Euler-Bernoulli beam and then sized using fully stressed design techniques for isotropic materials. As computers became more powerful in the 90's, finite element analysis allowed for accurate calculations involving complex cross-sections with non-isotropic material properties. While the results from finite element analysis are valuable in the design of complex structures, they are still time consuming. A simple yet complete beam theory would drastically reduce computational effort via a reduction in the number of elements, but an adequate beam model did not exist before Hodges' work on his intrinsic beam theory [11]. With continuing refinement and validation, a number of structural specialists have developed successful FEM beam formulations based on Hodges' theory with an eye towards helicopter rotor design applications [12–19]. Recent strain-based methods have been applied to the analysis and design of various equivalent-beam wing structures [20, 21]. Geo-

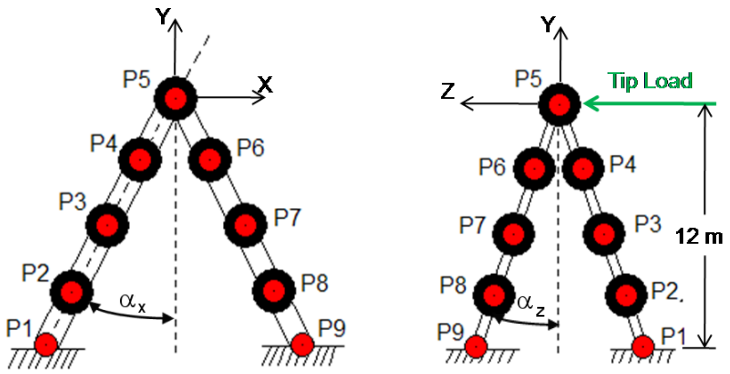

(a) Planform (b) View looking forward

Figure 1.2: Planform and view looking forward of joined-wing consisting of eight beam elements.

metrically Exact Beam Theory (GEBT) is an alternate beam element formulation with mixed displacement and force variables (as opposed to strain variables). Hodges' intrinsic beam theory incorporates all possible geometric nonlinear coupling combinations including geometric bend-twist coupling reported by Blair and Stritz [10]. That development motivated Yu in the broader development of GEBT with the goal of supporting gradient-based design optimization of slender aeroelastic wing concepts.

At the same time, Park et al. developed an optimization scheme for linear [5] and nonlinear [6] joined-wing structures based on equivalent static loads. Simply put, the displacements from the nonlinear analysis are used to develop a load vector that yields the same set of displacements when applied to a linear stiffness matrix. This two-step method starts with the converged solution of the nonlinear structural system, then applies a linear approximation technique to the current design. The equivalent load vector, or equivalent static loads (ESL), are then used in the linear response optimization until convergence is achieved. The entire process then repeats until the equivalent static loads for two consecutive nonlinear evaluations have converged.

The effort reported in this thesis document is a combination of GEBT and ESL as developed by Yu and Park respectively. A current limitation of this implementation of GEBT is the inability to accommodate loads applied to the wing tip beyond the wing joint. Therefore, only a design where the wings are joined at the wing tip is considered.

Load conditions will include only static vertical loads applied to the joint at the wing tip.

The goals of this research are first to develop a pilot application of the merger of GEBT and ESL. This merger leads to the second goal, which is to demonstrate the utility of GEBT in a computationally efficient design optimization process of a joined-wing concept using the method of equivalent static loads. The simplest possible realization which will exhibit geometric bend-twist coupling in a joined wing is shown in Fig. 1.2. Second, show that a low degree of freedom model of the joined wing is capable of capturing geometric bend/twist coupling exhibited in the joined-wing design. This thesis reports on the success of this demonstration. GEBT will continue to be developed in a series of steps that increase its usefulness in a computationally efficient aeroelastic design optimization process applied to highly flexible concepts.

II. Background

This research relies on three main bodies of work as foundational material. The first is the joined-wing design itself. The second is Geometrically Exact Beam Theory and its associated Variational Asymptotic Method and Variational Asymptotic Beam Section theories for analysis of beam elements. Third, Equivalent Static Loads will be discussed as a means of reducing computational effort to solve nonlinear structural optimization problems.

2.1 The Joined-Wing Aircraft

The joined-wing aircraft design is not a new concept within the history of manned flight. The novelty of the joined-wing is that the tools necessary to analyze the complex structural and aerodynamic properties were not available until the mid to late 1980's. History's first known successful flight of a joined-wing design was made by Reinhold Platz in 1922 [1]. The Platz joined-wing glider featured two wings joined at the tip, with the split upper forward wing being used to control both pitch and roll by the pilot. The lower aft wing was fixed and supplied most of the lift as shown in Fig. 2.1.

Other designers experimented with the joined-wing, but it wasn't until Wolkovitch was granted his patent in 1982 and presented an overview of the design's merits that aircraft designers began to consider the configuration as feasible [2]. Wolkovitch's patent application drawing is shown in Fig. 2.2. Several advantages are attributed to the joined-wing design when compared to a conventional aircraft design, including light weight, high stiffness, low induced and parasite drag, direct lift control, and good stability and control [3].

These advantages have since prompted much research into the joined-wing design. Structural optimization of the joined-wing design was investigated by Gallman and Kroo in 1996. They used two structural design methods: one a fully stressed design and the second a minimum weight design [4]. They concluded that the fully stressed design using nonlinear analysis tools approximates the minimum weight structure very well with a time savings in computational effort. More recently, the Air Force Research Laboratory (AFRL) has shown interest in the joined-wing design concept as a surveillance platform

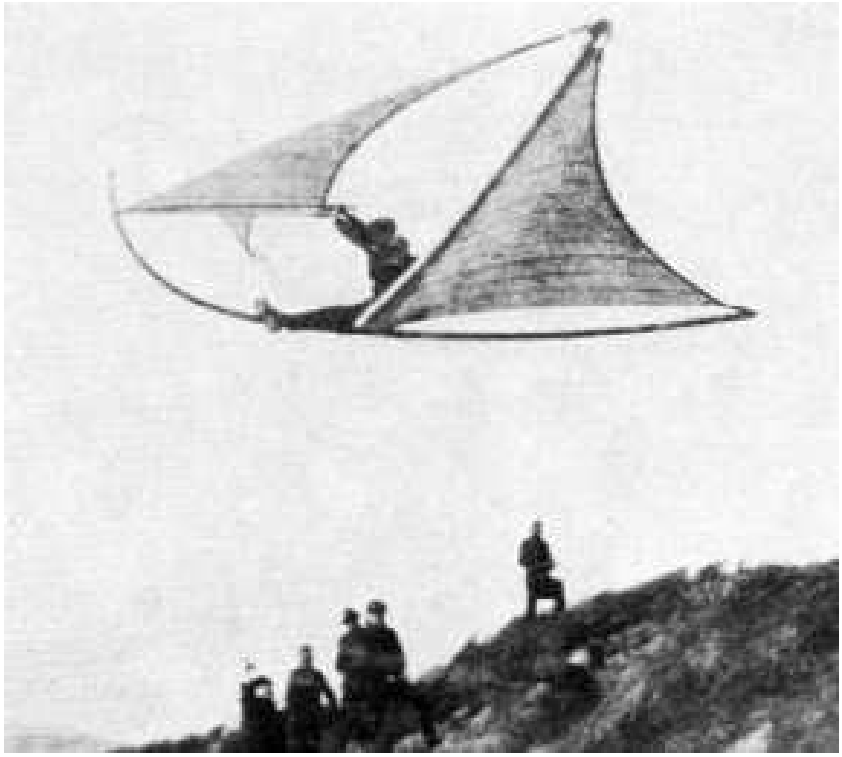

Figure 2.1: 1922 Platz glider [1]

with long range and endurance as key performance parameters. Blair and Canfield developed an integrated design method for the joined-wing aimed at merging the aerodynamic and structural designs into one all encompassing process [22]. They concluded that the geometric nonlinearities inherent in the joined-wing require a nonlinear analysis for loads that result in large deformations. In that vein, numerous studies have been performed on the joined-wing using the finite element method, with models having as many as 3,000 elements being considered for a single nonlinear analysis on a half span model [6].

2.2 Geometrically Exact Beam Theory (GEBT)

The most fundamental aspect of elasticity is Hooke's Law, which in 1D form is

$$F = -kx \tag{2.1}$$

where k is the stiffness of the element, x is the displacement of the element, and F is the axial force applied to the element. When expanded beyond the 1D axial problem,

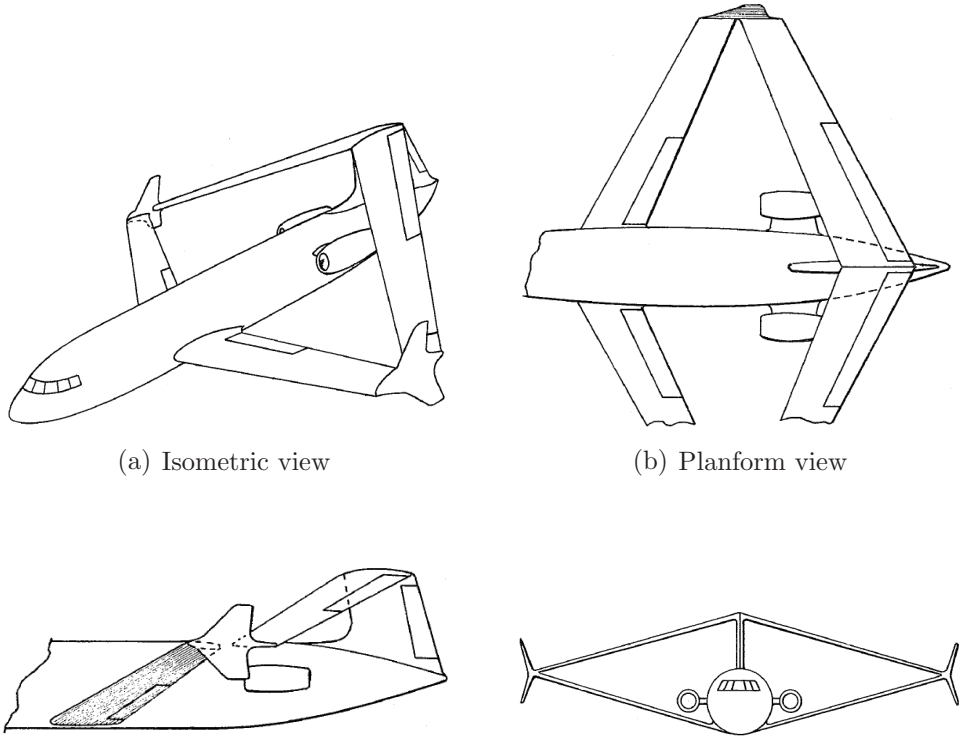

(a) Isometric view

(b) Planform view

(c) Side view

(d) Front view

Figure 2.2: Joined-wing aircraft design proposed by Wolkovitch in his patent application. [2]

application of Euler-Bernoulli beam theory considers only a 4x4 stiffness matrix due to the selection of displacement and slope at the two nodes as the degrees of freedom under consideration. The assumption that planar surfaces remain in plane and normal to the longitudinal axis under deformation allows shear deformation to be neglected. Timoshenko expands on the Euler-Bernoulli beam theory by considering planar surfaces which remain plane, but not normal to the longitudinal axis of the beam element. Inclusion of the angle of shearing in the two directions of the beam element cross section increases the degrees of freedom to 6, resulting in a 6x6 stiffness matrix.

With an eye towards helicopter rotor blade design, Hodges began an investigation into beam theory in the mid 1980's that would eventually result in a generalized beam theory that is not burdened by several assumptions that are often required when conducting analysis of long, slender beams. He presented his mixed variational formulation beam theory in 1989 and notes that his work is the assemblage of three sets of previous works [11].

First is a kinematical basis for deformed beams. Danielson and Hodges used the polar decomposition theorem to obtain an accurate yet compact expression for the strain in a beam or rod experiencing large deflections [23]. The polar decomposition theorem facilitates this by decomposing the total deformation of any element into a pure strain and a pure rotation. Danielson and Hodges concluded that strain components are explicit functions of position within the cross section and implicit functions of the length along the beam axis x_1. There are a total of seven implicit functions, dependent on strain (γ_{11}) and transverse shear (γ_{12} and γ_{13}) of the reference line, bending strains (κ_2 and κ_3), and warp amplitude (ψ). In 1988, Danielson and Hodges developed both an intrinsic and explicit version of their beam theory [24]. The intrinsic beam theory is for static, nonlinear beams and is expressed in terms of the generalized strains described in Ref. [23] and is applicable when generalized forces and moments applied at the ends of the beam are known. The explicit theory by contrast is applicable when the generalized transverse and rotational displacements are known in conjunction with the warp amplitude (u_i, θ_i, and ψ respectively). Thus, Danielson and Hodges put forward theories that addressed the global kinematics of deformed beams using Cartesian tensors and matrix notation,

eliminating the need for curvilinear coordinate systems and reducing the size of the equations required.

Second, Atilgan and Hodges expanded on Parker's 1979 work in Ref. [25]. Parker showed that, using a perturbation procedure based on scaling of the axial variations, St. Venant's semi-inverse solutions for bending and torsion of rods and beams could be used to describe beams undergoing large displacements and rotations. Parker also stated that the classical solution for beam flexure is composed of two parts: a bending solution and a varying curvature along the axis of the beam. The use of asymptotic analysis, such as that used by Parker, allowed Atilgan and Hodges to conclude a linear 2D cross-section deformation analysis can be used to determine the appropriate stiffness for use in the 1D nonlinear beam global analysis [26].

Third, Reissner derived strain measures from internal beam forces and virtual work using an intrinsic analysis [27, 28]. This intrinsic analysis supports the later work by Danielson and Hodges which was based strictly on kinematics [23]. The agreement between the two approaches indicates that the general equations to describe strain measures are now available to the engineering community.

Building upon the three principles just described, Hodges applies a variational approach using Hamilton's principle that concludes with a mixed variational formulation for a geometrically exact beam theory [11]. The advantages with this formulation lie in the compact matrix form in which the theory is expressed, along with the absence of any approximations in the geometry of the deformed elements along the reference line (i.e. beam axis) or the cross section. Hodges also notes that the mixed formulation allows the use of simple shape functions consisting of constant values for field variables along the beam element. Discontinuities in field variables between elements are also possible, which eliminates the requirement of numerical quadrature over the elements. Instead, a 1x1 quadrature is performed at the center of each element to obtain an approximate stiffness, mass, etc.

Hodges' theory has been expanded to use the Timoshenko approach by including the shear terms, but still relies on the presence of small strains while not restricting displacements and rotation variables. This trait is due to the derivation of the theory from

geometrically nonlinear, three dimensional elasticity theory. In the last two decades the geometrically exact canonical equations of motion for beams have been presented separately by Borri and Mategazza, Hodges, and Bauchau and Kang [11, 29, 30]. This body of work lends itself to expressing energy in terms of variables compatible with large global displacements and rotations. Hodges' Geometrically Exact Beam Theory (GEBT) requires the cross-sectional elastic constants, EI, GJ, etc. as the inputs to the equations used for solving for the displacements and rotations. While this approach allows for the use of complex beam structures, it leaves the user with the task of providing the cross-sectional constants before the calculation can proceed. In GEBT, the stiffness matrix for a prismatic isotropic material is

$$C = \begin{pmatrix} EA & 0 & 0 & 0 & 0 & 0 \\ 0 & GA_{xx} & 0 & 0 & 0 & 0 \\ 0 & 0 & GA_{zz} & 0 & 0 & 0 \\ 0 & 0 & 0 & GJ & 0 & 0 \\ 0 & 0 & 0 & 0 & EI_{xx} & 0 \\ 0 & 0 & 0 & 0 & 0 & EI_{zz} \end{pmatrix} \tag{2.2}$$

where EA is the axial rigidity, EI_{xx} is the bending rigidity about the global X-axis, EI_{zz} is the bending rigidity about the global Z-axis, GJ is the torsional rigidity, GA_{xx} is the shear rigidity in the global X-direction, and GA_{zz} is the shear rigidity in the global Z-direction. The 1D displacement vector $\boldsymbol{\epsilon}$ is defined as

$$\epsilon = \lfloor \gamma_{11} \; 2\gamma_{12} \; 2\gamma_{13} \; \kappa_1 \; \kappa_2 \; \kappa_3 \rfloor^T \tag{2.3}$$

where γ_{11} is the extensional strain of the reference line, $2\gamma_{12}$ and $2\gamma_{13}$ are the transverse shear strain measures, and κ_i are the twist and bending generalized strain measures [12]. The force vector applied to the beam is

$$F = \lfloor F_1 \; F_2 \; F_3 \; M_1 \; M_2 \; M_3 \rfloor^T \tag{2.4}$$

where F_i is the force in the X, Y, or Z direction, respectively, and M_i is the moment about the X, Y, or Z-axis. Using the mixed formulation in GEBT, the 1D constituitive relation for isotropic materials is

$$\begin{Bmatrix} F_1 \\ F_2 \\ F_3 \\ M_1 \\ M_2 \\ M_3 \end{Bmatrix} = \begin{bmatrix} EA & 0 & 0 & 0 & 0 & 0 \\ 0 & GA_{xx} & 0 & 0 & 0 & 0 \\ 0 & 0 & GA_{zz} & 0 & 0 & 0 \\ 0 & 0 & 0 & GJ & 0 & 0 \\ 0 & 0 & 0 & 0 & EI_{xx} & 0 \\ 0 & 0 & 0 & 0 & 0 & EI_{zz} \end{bmatrix} \begin{Bmatrix} \gamma_{11} \\ 2\gamma_{12} \\ 2\gamma_{13} \\ \kappa_1 \\ \kappa_2 \\ \kappa_3 \end{Bmatrix} \tag{2.5}$$

There are at present two implementations of GEBT in code. Yu has made available a Fortran 90/95 based version that as of this writing is only capable of addressing linear static problems. The GEBT implementation used in this research is a prototype Mathematica code that allows nonlinear analysis of the joined-wing. The inputs to the GEBT implementation are the applied load, the number of elements, the total length of all beam elements, and the cross sectional properties for each element described in Eq. (2.5). The GEBT implementation returns forces, moments, displacements, and rotations for each element, as well as the reaction forces at the constrained nodes (fore and aft wing roots in the case of this research effort). The forces, moments, displacements, and rotations are reported at the center of each beam element. It is possible to extrapolate nodal displacements and rotations by starting at the wing root and using a linear interpolation

$$u_{node\ i} = u_{node\ i-1} + 2(u_{elem\ i} - u_{node\ i-1}) \tag{2.6}$$

where $u_{node\ i}$ is the nodal displacement, $u_{node\ i-1}$ is the nodal displacement at the previous node, and $u_{elem\ i}$ is the displacement at the mid section of the beam element.

2.3 Variational Asymptotic Beam Sectional Analysis (VABS)

The Variational Asymptotic Beam Sectional Analysis (VABS) is a method which uses cross sectional properties in a 2D analysis based on the variational asymptotic

method (VAM). Some of the background on VABS is described in Section 2.2. The 1D nonlinear beam analysis and the 2D cross-sectional analysis were derived in the context of the VAM developed by Berdichevskii in 1976 [31]. Berdichevskii dealt with nonhomogeneous anisotropic beams. Hodges et al. extended the work to include prismatic beams [7]. The application of VAM to beam theory requires that the 3D strain energy of a beam is asymptotically reduced in two distinct steps to yield a 1D beam strain energy equation. This 1D strain energy equation is decoupled from the 2D cross-sectional analysis, allowing the complex 3D problem to be split into two separate problems. Popescu and Hodges offer a definition of 'asymptotically correct':

> By asymptotically correct, we mean that an expansion of the approximate solution in terms of a small parameter agrees with a similar expansion of the exact solution up to a certain order in the small parameter [32].

Yu et al. expanded Hodges' work to handle Timoshenko like modeling of initially curved and twisted beams to address short wavelength motions caused by shear effects [9]. At the same time, he updated an engineering software package known as VABS III, hereafter called VABS, to include the latest refinements to Hodges' model. VABS is a computer program based on the VAM which allows users to analyze composite beam cross sections accurately and quickly using finite element methods with the processing power found in the average desktop computer [33].

An input file is required that describes the cross section, material properties, coordinate transformation, and forces and moments applied to the element under consideration [34]. The cross section is defined by a set of nodes that refer only to points within the cross section, and have no relation at all to the nodes depicted in Fig. 1.2. For this research, VABS is used to supply highly reliable calculations of the nonlinear stresses resulting from the forces and moments calculated in the nonlinear analysis by GEBT [8].

2.4 Calculation of Equivalent Static Loads

The geometric nonlinearity of the joined-wing leads the designer down a difficult path. A linear optimization is not likely to be adequate, or perhaps even safe as noted by Kim et al. [6]. During cruise and maneuvering flight, Kim et al. showed that the

maximum tip von Mises stress in a geometric nonlinear analysis could be as much as 10 times the maximum von Mises stress in a linear analysis, while displacements in the nonlinear case were 5 times the maximum displacements in the linear analysis. From this it is clear that a linear analysis, while fairly simple to implement, is not sufficient when considering design of a structure that exhibits highly nonlinear responses.

The alternative to the linear response optimization has been a full nonlinear response optimization. The major drawback to any nonlinear problem lies in the large computational effort involved in calculating a solution. This increase in effort is due to the numerical approach of convergence to a solution using multiple intermediate linearizations. Sensitivity calculations in the optimization contribute to the total effort as well. Analytic sensitivity calculation and the finite difference method are the two common approaches to obtaining sensitivities. Although computationally expensive, finite difference techniques are easy to implement. Analytical evaluations of sensitivity have advantages and drawbacks that are opposite of the finite difference method. Analytical means are cheap in terms of computational effort, but are often either very complex or simply undetermined in large, complex nonlinear problems. With the use of the finite difference method, it follows that any increase in the number of design variables will directly affect the length of time required to perform each iteration in the optimization process. In an effort to circumvent large numbers of nonlinear operations, a linear approximation to the nonlinear response optimization problem has been proposed.

Lee, et al. define equivalent loads (EL) as loads for linear analysis which generate the same response fields as those of nonlinear analysis [5]. In the optimization problem in this research, equivalent static loads (ESL) are used to define a linear approximation of the displacement field resulting from a nonlinear response to an applied load. The ESL are then passed to the optimization routine allowing a linear response optimization to be performed, resulting in less computational effort required to determine a solution to the optimization problem. After convergence of the linear approximation, the design is reevaluated using a nonlinear analysis on the linear approximation design and checked for convergence. When the equivalent static loads are no longer changing from one iteration to the next, the optimization problem has converged.

2.4.1 ESL for Displacement Constraints. The first step in calculating an equivalent static load is to perform a nonlinear analysis

$$\boldsymbol{K(b)z_n = f} \tag{2.7}$$

where $\boldsymbol{K(b)}$ is the nonlinear stiffness matrix, $\boldsymbol{z_n}$ is the nonlinear nodal displacement vector, and $\boldsymbol{f}$ is the applied load vector. Due to the dimensional reduction of the 3D beam problem when using VAM, the cross sectional analysis becomes a linear 2D problem involving the cross sectional stiffness properties [34]. This is different than the approach described by Lee and Kim where the stiffness matrix is a function of both the design variables $\boldsymbol{b}$ and the displacement vector $\boldsymbol{z_n}$ [5, 6]. Equivalent static loads $\boldsymbol{f^z_{eq}}$ for displacements are computed from

$$\boldsymbol{f^z_{eq} = K_L(b)z_n} \tag{2.8}$$

where $\boldsymbol{K_L(b)}$ is the linear stiffness matrix, $\boldsymbol{z_n}$ is from the nonlinear analysis from Eq. (2.7).

2.4.2 ESL for Stress Constraints. Similarly, the equation for the equivalent static load (ESL) for stresses $\boldsymbol{f^\sigma_{eq}}$ is

$$\boldsymbol{f^\sigma_{eq} = K_L(b)z^\sigma_n} \tag{2.9}$$

where $\boldsymbol{z^\sigma_n}$ is the displacement vector calculated from the nonlinear stress result described [5]. In the research presented here, an alternate means of calculating the equivalent stresses is used. This alternate approach uses the same equivalent static loads vector calculated for the displacement constraint case and is presented in MSC Nastran's implementation of the ESL routine [35]. The equivalent static load for displacement does not produce the same set of stresses as the nonlinear analysis, so the stress ratio correction from Lee, et al. is retained [5]. The stress ratio $\boldsymbol{\alpha}$ is defined as

$$\boldsymbol{\alpha = \frac{\sigma_{NL-VM}}{\sigma_{L-VM}}} \tag{2.10}$$

which is calculated prior to entering the linear response optimization. The von Mises stress from nonlinear analysis is $\boldsymbol{\sigma_{NL-VM}}$, and the von Mises stress from the linear approximation using equivalent static loads is $\boldsymbol{\sigma_{L-VM}}$. In the optimization routine, it is applied to the linear stress calculation using linear Euler-Bernoulli beam theory. The stress vector approximation $\boldsymbol{\sigma'_{L-VM}}$ is defined as

$$\boldsymbol{\sigma'_{L-VM}} = \boldsymbol{\alpha}\ \boldsymbol{\sigma_{L-VM}} \tag{2.11}$$

where $\boldsymbol{\sigma_L}$ is the stress vector calculated using $\boldsymbol{f^z_{eq}}$ as the load before the correction factor $\boldsymbol{\alpha}$ is applied. The vector $\boldsymbol{\sigma'_{L-VM}}$ is used to determine the von Mises stress in each element. These values are then used in stress constraint violations such that

$$\boldsymbol{\sigma'_{L-VM}} \leq \boldsymbol{\sigma^{VM-allowable}} \tag{2.12}$$

where $\boldsymbol{\sigma^{VM-allowable}}$ is the von Mises stress constraint defined in the optimization problem.

III. Methodology

3.1 Model Definition

The model is described in Cartesian coordinates using a global right hand coordinate system with the wing tip as the origin. The stream wise direction (the direction the airflow would go if the vehicle were in flight) is along the positive global X-axis. The positive Y-axis is directed out the span through the wing tip, and is normal to the longitudinal axis of the aircraft. The positive Z-axis is directed in the upward direction. The beam elements are oriented so that the area exposed to the free stream flow is the height of each beam multiplied by its length as shown in Fig. 3.1.

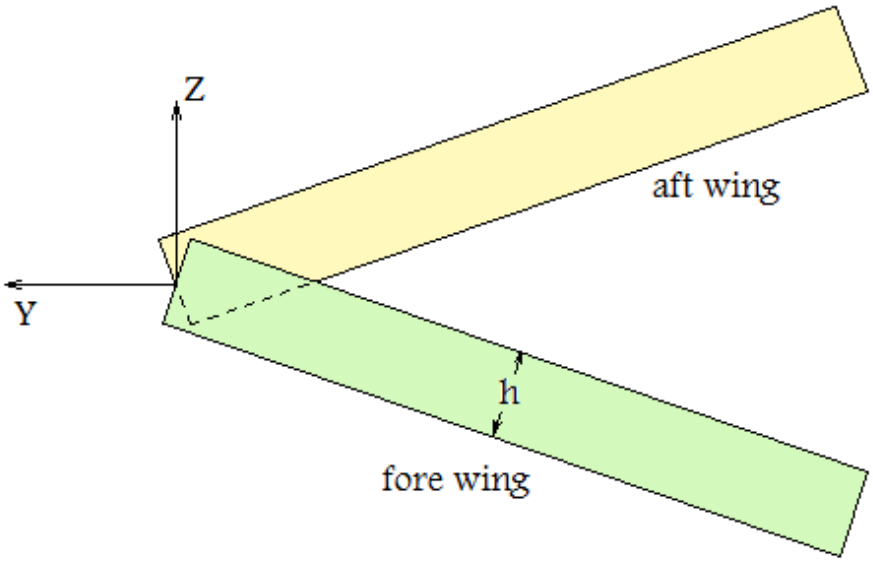

Figure 3.1: View looking aft showing beam element orientation (not to scale)

Wolkovitch states that the effect of joint location has a great impact on the efficiency gains claimed by joined-wing aircraft [3]. He estimates that joint locations from 60% to 100% of the wing span should be evaluated in order to truly find an optimum design. Due to a limitation of the implementation of GEBT used in this research, there is no consideration of a joined wing with any structure beyond the wing joint itself. This research considers both 8 and 16 beam element models. Regardless of the number of elements, the location of the wing tip and the fore and aft wing root locations does not change. The coordinates for the wing roots are shown in Table 3.1.

Table 3.1: Simple Joined-Wing Model Configuration

Dimension	Value (m)
$x(fore\ root)$	-7.173
$y(fore\ root)$	-12.000
$z(fore\ root)$	-3.215
$x(aft\ root)$	7.173
$y(aft\ root)$	-12.000
$z(aft\ root)$	3.215
c chord	1.500
h height	0.150
t_s skin thickness	0.015
t_w web thickness	0.015

The model under examination here is a simple box beam of isotropic material as shown in Figure 3.2, and the cross sectional elastic constants for a thin walled box beam are

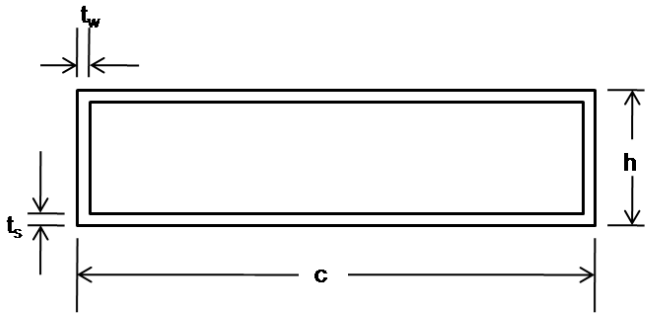

Figure 3.2: Cross section of simple box beam

$$EA = 2E[ct_s + (h - 2t_s)t_w] \tag{3.1}$$

$$EI_{xx} = E\left[\frac{ch^3}{12} - \frac{(c - 2t_w)(h - 2t_s)^3}{12}\right] \tag{3.2}$$

$$EI_{zz} = E\left[\frac{hc^3}{12} - \frac{(h - 2t_s)(c - 2t_w)^3}{12}\right] \tag{3.3}$$

$$GJ = \frac{4G\overline{A}^2}{\int_0^s \frac{1}{t} ds} \tag{3.4}$$

$$GJ = \frac{2Gc^2h^2}{(\frac{c}{t_s} + \frac{h}{t_w})} \tag{3.5}$$

$$GA_{xx} = 2Gct_s \tag{3.6}$$

$$GA_{zz} = 2G(h - 2t_s)t_w \tag{3.7}$$

where c is the chord, h is the height, t_s is the thickness of the top and bottom skins, and t_w is the thickness of the web. For the simple geometry under consideration, Eqs. (3.1) - (3.7) are used to determine the cross-sectional properties. Equation (3.4) is the general form of the torsion constant equation for thin walled sections of any shape [36]. Equation (3.5) is the form used in the calculations in this research as applied to a thin walled box beam. For more complex cross sections, VABS is well suited to performing this task but is not required for this simple cross section.

While it is possible to apply loads to any node in the model, the loads are limited here to static loads at the wing tip in the positive global Z-axis direction. A small 500 N load allows comparison of displacement results from linear and nonlinear analyses to ensure correlation early in the setup of the optimization problem. The design applied tip load, $P_{applied} = 33{,}670$ N, is that described by Blair in Ref. [10]. Table 3.2 shows the force and moment results and Table 3.3 shows the displacement results for the 500 N test case for both the nonlinear solution using GEBT and a linear solution using Euler-Bernoulli beam theory.

The element forces and moments are in the local beam coordinate system while the nodal displacements and rotations are in the global coordinate system. There is excellent agreement between these two sets of data. This research focuses on the displacement term u_3 at node 5, which is where the displacement constraint defined in Eq.(3.10) is enforced. The nonlinear solution from GEBT is 0.001132 m. When the equations in GEBT are linearized, the tip deflection is still 0.001132 m. The linear solution using Euler-Bernoulli is 0.001141 m, a difference of 0.8%. The linear beam model used is not a Timoshenko, which means the shear correction terms are not considered. The cause of this difference is not known at this time, although the nonlinear and linear solutions in GEBT are the same, so linearization of GEBT does not seem to be the cause.

Larger loads are expected to result in nonlinear deformation when applied to the system. Furthermore, GEBT should yield a nonlinear response while the Euler-Bernoulli

Table 3.2: 500 N test load force and moment results from nonlinear and linear analysis with all elements set to initial design variable values as given in Table 3.1

Analysis	Element	F_1	F_2	F_3	M_1	M_2	M_3
			(N)			(N-m)	
GEBT	1	758	-437	-24.4	128	233	-5450
	2	758	-437	-24.4	128	145	-3880
	3	758	-437	-24.4	128	57	-2310
	4	758	-437	-24.4	128	-30	-745
	5	-758	437	-24.5	-128	30	-745
	6	-758	437	-24.4	-128	-57	-2310
	7	-758	437	-24.4	-128	-145	-3880
	8	-758	437	-24.4	-128	-232	-5450
Euler-Bernoulli	1	758	-437	-24.4	128	233	-5450
	2	759	-437	-24.4	128	145	-3880
	3	759	-437	-24.4	128	57	-2310
	4	759	-437	-24.4	128	-30	-745
	5	-759	437	-24.5	-128	30	-745
	6	-759	437	-24.4	-128	-57	-2310
	7	-759	437	-24.4	-128	-145	-3880
	8	-758	437	-24.4	-128	-232	-5450

solution remains linear when the same tip load is applied to both models. Table 3.4 shows the force and moment results while Table 3.5 shows the displacement and rotation results for $P_{applied}$ = 33,670 N for both the nonlinear solution using GEBT and a linear solution using Euler-Bernoulli beam theory.

Agreement between linear and nonlinear analysis at $P_{applied}$ = 33,670 N is shown in Table 3.5. The nonlinear response is highlighted best by examining the response in the u_2 direction and rotation θ_2 at node 5 in Table 3.5. Although still very small, the value predicted by the nonlinear solver for θ_2 is now on the order of 10^{-6}, an increase of 10 orders of magnitude over the numerically zero result for the same value in the linear analysis. Likewise, the u_2 deflection has appeared and is the same order of magnitude as the other nodes in the nonlinear case, where the linear solution predicts no displacement in the global Y axis. The displacement used in the optimization, u_3 at the wing tip (node 5), is 76.26 mm in the nonlinear analysis and 76.84 mm in the linear analysis, a 0.8% difference. Closer inspection of the data shows that the behavior of the displacements in

Table 3.3: 500 N test load displacement and rotation results from nonlinear and linear analysis with all elements set to initial design variable values as given in Table 3.1

Analysis	Node	u_1	u_2	u_3	θ_1	θ_2	θ_3
		(μm)			(rad)		
GEBT	2	-42	-2	105	5.86e-05	-1.85e-05	2.28e-05
	3	-156	-7	381	9.86e-05	-2.46e-05	4.09e-05
	4	-317	-8	749	1.20e-04	-1.85e-05	5.43e-05
	5	-501	0	1132	1.23e-04	-4.99e-10	6.31e-05
	6	-317	8	749	1.20e-04	1.84e-05	5.43e-05
	7	-156	7	381	9.87e-05	2.46e-05	4.09e-05
	8	-42	2	105	5.86e-05	1.84e-05	2.28e-05
Euler-Bernoulli	2	-43	-3	110	5.79e-05	-1.83e-05	2.29e-05
	3	-158	-8	388	9756e-05	-2.44e-05	4.10e-05
	4	-320	-9	757	1.19e-04	-1.83e-05	5.44e-05
	5	-505	0	1141	1.22e-04	-1.70e-18	6.31e-05
	6	-320	9	757	1.19e-04	1.83e-05	5.44e-05
	7	-158	8	388	9.75e-05	2.44e-05	4.10e-05
	8	-43	3	110	5.79e-05	1.83e-05	2.29e-05

the u_2 and u_3 directions as well as F_3 and M_1 show a noticeable and expected departure from linear behavior predicted by Euler-Bernoulli.

3.2 Material and Geometric Properties

The model in this research is made of isotropic prismatic aluminum beams. The cross section is a thin-walled box with four variables as shown in Fig. 3.2. Material properties used were for aluminum, with a fixed Young's modulus E of 70.0 GPa and shear modulus G of 26.31 GPa. The stress criteria used were von Mises stress, defined as

$$\sigma_{VM} = \sqrt{\frac{(\sigma_{11} - \sigma_{22})^2 + (\sigma_{22} - \sigma_{33})^2 + (\sigma_{33} - \sigma_{11})^2 + 6(\sigma_{12}^2 + \sigma_{23}^2 + \sigma_{31}^2)}{2}} \tag{3.8}$$

where σ_{ij} are the components of the 3D stress tensor. Equation (3.8) can be applied to both the nonlinear and linear stresses obtained from GEBT and Euler-Bernoulli, respectively. For the stresses computed using Euler-Bernoulli linear beam theory, the von Mises stresses are calculated at both ends of each beam element at all four corners. These points are shown as gray triangles in Fig. 3.3. In the Mathematica implementation

Table 3.4: 33,670 N load force and moment results from nonlinear and linear analysis with all elements set to initial design variable values as given in Table 3.1

Analysis	Element	F_1	F_2	F_3	M_1	M_2	M_3
			(kN)			(kN-m)	
GEBT	1	51.1	-29.5	-1.81	7.74	16.0	-366
	2	51.1	-29.4	-1.61	8.69	9.46	-261
	3	51.2	-29.4	-1.49	9.02	3.64	-155
	4	51.2	-29.3	-1.44	9.04	-1.75	-50.1
	5	-50.9	29.6	-1.85	-8.18	2.30	-50.2
	6	-50.9	29.6	-1.80	-8.21	-4.12	-156
	7	-50.9	29.5	-1.67	-8.56	-10.1	-262
	8	-51.0	29.4	-1.48	-9.52	-1.53	-368
Euler-Bernoulli	1	51.1	-29.4	-1.62	8.54	15.5	-367
	2	51.1	-29.5	-1.63	8.53	9.65	-262
	3	51.1	-29.5	-1.63	8.54	3.81	-156
	4	51.1	-29.6	-1.63	8.54	-2.01	-50.2
	5	-51.1	29.6	-1.63	-8.54	2.01	-50.2
	6	-51.1	29.5	-1.63	-8.54	-3.81	-156
	7	-51.1	29.5	-1.63	-8.54	-9.65	-262
	8	-51.1	29.4	-1.62	-8.54	-15.5	-367

Table 3.5: 33,670 N load displacement and rotation results from nonlinear and linear analysis with all elements set to initial design variable values as given in Table 3.1

Analysis	Node	u_1	u_2	u_3	θ_1	θ_2	θ_3
			(mm)			(rad)	
GEBT	2	-2.85	-0.18	7.23	3.94e-03	-1.39e-03	1.49e-03
	3	-10.5	-0.61	25.9	6.58e-03	-1.75e-03	2.72e-03
	4	-21.3	-0.80	50.6	8.02e-03	-1.26e-03	3.65e-03
	5	-33.8	-0.34	76.3	8.31e-03	-2.27e-06	4.25e-03
	6	-21.3	0.34	50.3	8.19e-03	1.22e-03	3.67e-03
	7	-10.5	0.32	25.4	6.71e-03	1.56e-03	2.79e-03
	8	-2.86	0.09	6.97	3.94e-03	1.09e-03	1.58e-03
Euler-Bernoulli	2	-2.91	-0.17	7.39	3.90e-03	-1.23e-03	1.54e-03
	3	-10.6	-0.51	2.61	6.57e-03	-1.64e-03	2.76e-03
	4	-21.5	-0.59	51.0	8.00e-03	-1.23e-03	3.67e-03
	5	-34.0	0.00	76.8	8.21e-03	-1.21e-16	4.25e-03
	6	-21.5	0.59	51.0	8.00e-03	1.23e-03	3.67e-03
	7	-10.6	0.51	26.1	6.57e-03	1.64e-03	2.76e-03
	8	-2.91	0.17	7.39	3.90e-03	1.23e-03	1.54e-03

of GEBT used in this research, stresses are not returned directly. As mentioned earlier, the GEBT outputs are forces and moments. These forces and moments are calculated at the center of each beam element in the beam element's local coordinate system, relieving the user of the need to apply a transformation from the global to local coordinate system.

Calculation of the 3D nonlinear stresses and strains are computed by the current Fortran implementation of VABS. The inputs for VABS are the description of the cross sectional geometry, material properties, and forces and moments applied to the element. VABS calculates all cross sectional properties for the stiffness matrix prior to analysis, and returns 3D stress and strain tensors at any point in the cross section desired by the user at the midpoint of the beam element. In this research, a cross section for the thin wall box beam is defined using 20 nodes which are grouped into four elements. These elements comprise the top and bottom skins and the fore and aft webs. These elements of the cross section are shown in Fig. 3.4. Each element is defined by eight nodes, six of which are shared with other elements. As a result, the stress and strain outputs are calculated at each node for each element, resulting in 32 outputs for stress recovery, not 20. The stresses reported at the same node twice are averaged to give a single stress tensor. The cross section is shown as the shaded section with green circles denoting the stress recovery points used in the von Mises stress calculations in Fig. 3.3. The corners shown at the midpoint cross section relate to the ends of the beam for comparison purposes. To allow comparison between the GEBT/VABS nonlinear and the Euler-Bernoulli linear stresses, the von Mises stresses obtained from the linear analysis at the ends of the beam are averaged. This approach works due to the constant force and linear moment distributions across a given element. These averaged linear von Mises stresses compare very well to VABS for the 500 N linear test case at the midpoint cross-section of each beam element.

3.3 Structural Optimization Problem

For each beam element the chord and height of the wing box as well as the thickness of the skins (upper and lower surfaces) and webs (fore and aft surfaces) are all design variables as shown in Fig. 3.2. If the design variables of the eight beams listed in Fig. 1.2

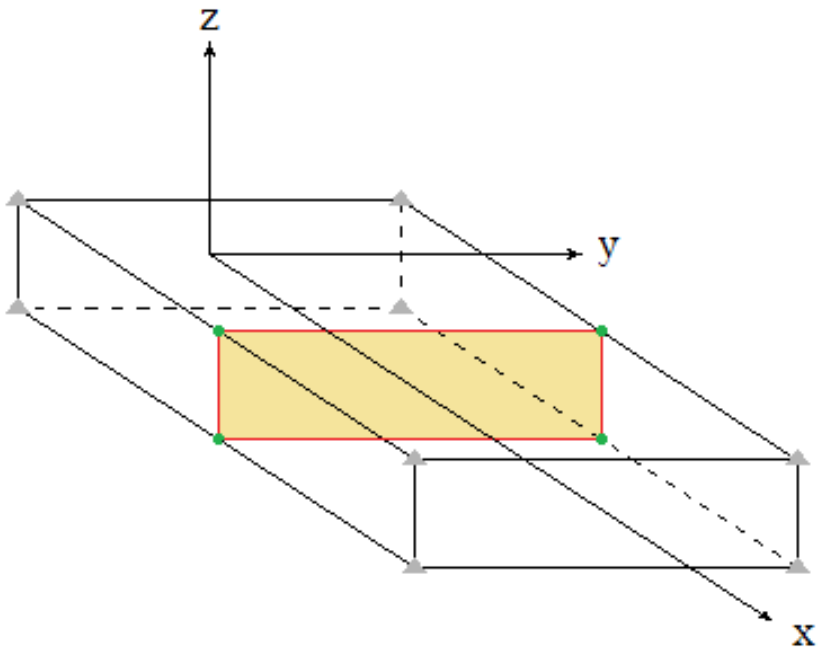

Figure 3.3: Simple box beam showing locations of von Mises stress calculations

are linked, there are only four design variables. In the case where each of the eight beam element's four design variables are independent of the others, there are thirty-two design variables. Upper and lower bounds were defined for each of the four design variables. It is important to note that the constraint on the height of the box beam is a percentage of the current value of the chord. As a result, this height constraint must be continuously updated in the optimization loop as values of the chord changes. If the height constraint is not updated, it is possible that the optimization will return a result that is inconsistent with this constraint. In the displacement optimization problem, vertical global Z-axis deflection at the wing tip is the design constraint. The values were either a direct result of the GEBT nonlinear analysis or Eq. (3.11) when using ESL. Although initially considered as two separate problems during development, the displacement and stress

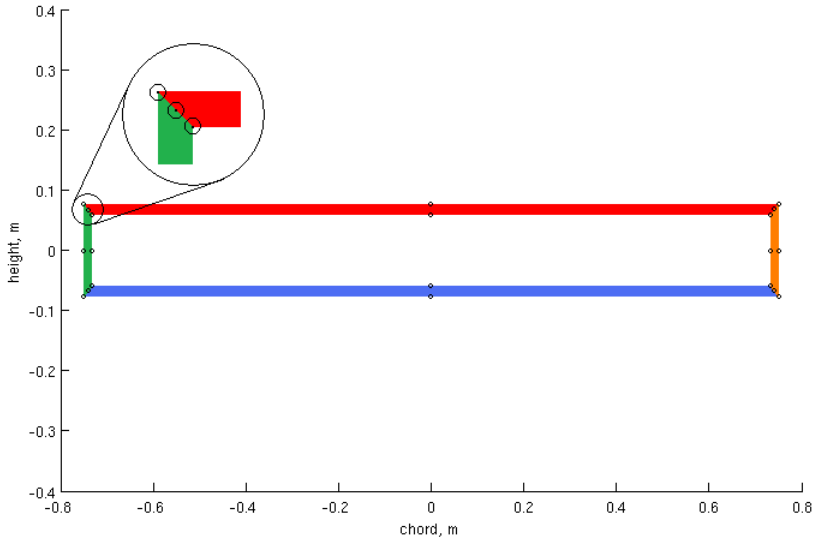

Figure 3.4: Cross section view showing nodes used by VABS to calculate stress recovery points.

constrained optimization problem is formulated as:

$$
\begin{aligned}
\text{Find} \quad & \boldsymbol{b} = \lfloor \boldsymbol{c}\ \boldsymbol{h}\ \boldsymbol{t_s}\ \boldsymbol{t_w} \rfloor^{\boldsymbol{T}} \\
\text{to minimize} \quad & \boldsymbol{M(b)} \\
\text{subject to} \quad & |u_{tip}| \leq u_{z-dir\ allowed} \\
& \boldsymbol{\sigma}_{VM} \leq \boldsymbol{\sigma}_{VM\ allowed} \\
& 0.500 \leq \boldsymbol{c} \leq 2.500 \text{ m} \\
& 0.05\ \boldsymbol{c} \leq \boldsymbol{h} \leq 0.15\ \boldsymbol{c} \text{ m} \\
& 0.005 \leq \boldsymbol{t_s} \leq 0.015 \text{ m} \\
& 0.005 \leq \boldsymbol{t_w} \leq 0.015 \text{ m}
\end{aligned}
\tag{3.9}
$$

The mass of the model with all values set to the initial design variables shown in Table 3.1 is 3764.8 kg. A MATLAB sequential quadratic programming (SQP) optimization routine is used for the optimization.

3.4 Integration between Mathematica and MATLAB

Research was performed in a Linux environment due to the need to call Mathematica from within the MATLAB code during the optimization process. A script used to handle writing the calculated cross-sectional properties EI, GJ, et al. to a text file. Mathematica is then called using a shell command and the Mathematica program (GEBT) is executed. GEBT initializes its variables, then reads the input files created by MATLAB to obtain cross-sectional data. Nonlinear analysis is then conducted, with displacement, rotation, force and moment resultants returned in a single matrix that is then written to a comma separated value (CSV) file. The MATLAB script resumes by reading the CSV file and transforming the Mathematica output into MATLAB format. The values returned from GEBT are at the mid point of each element, so a linear shape function is applied to determine nodal displacements and rotations using Eq. (2.6)

3.5 Nonlinear Optimization using GEBT

Two different approaches to the optimization problem are investigated. In the first approach, which will be referred to as GEBT, a full nonlinear response optimization is carried out using GEBT as the nonlinear solver. The second approach, which will be referred to as GEBT-ESL, is the linear response optimization using ESL in conjunction with the GEBT nonlinear solver. In the nonlinear response optimization, the optimization is driven by a full nonlinear analysis. The optimization starts with a nonlinear analysis of the model, defines upper and lower bounds on the design variables, and then hands the model off to SQP. The nonlinear analysis is completed by a Mathematica implementation of GEBT each time the objective and constraint equations are calculated within SQP using the current values of all design variables. The joined-wing analysis does not have explicit equations programmed that can be used to calculate

$$\frac{\partial\ u_{tip}(b)}{\partial\ b_i} \tag{3.10}$$

which is the partial derivative of the wing tip displacement with respect to each design variable. The gradient based search method employed by SQP requires a sensitivity anal-

ysis with respect to each design variable be performed on the current design, including each finite difference calculation used to determine the search direction.

The output from GEBT is then processed into terms that are used in the constraint equations for displacement and stress as shown in Fig 3.5(a).

3.6 Nonlinear Optimization using GEBT with ESL

The second approach investigated also uses the Mathematica implementation of GEBT for nonlinear analysis in an outer loop to determine displacements and von Mises stresses. However, a set of equivalent loads calculated with a linear stiffness matrix before beginning optimization is shown in Fig. 3.5(b) and is used in a linear design analysis. The equivalent loads are used with the current linear stiffness matrix to calculate a set of approximate nonlinear displacements from

$$\{d\} = [K_L(b)]^{-1}\{f_{eq}^z\} \tag{3.11}$$

where $\boldsymbol{d}$ is the displacement vector, $\boldsymbol{K_L(b)}$ is the linear stiffness matrix using the design variables of the current iteration, $\boldsymbol{b}$ is the vector of design variables, and $\boldsymbol{f_{eq}^z}$ is the equivalent static loads vector for displacements that was calculated in the outer loop. From the displacements $\boldsymbol{d}$, stresses are calculated using Euler-Bernoulli beam theory. The element stresses are then used to calculate the von Mises stress for each element using Eq. (3.8) Within the optimization inner loop, these approximate displacements and stresses will be used in the evaluation of the constraint equations in Eq. (3.10). Once SQP has converged to a solution, the results are returned to the outer loop, where the nonlinear analysis is performed again, and the process repeats until the convergence criteria,

$$\epsilon_{converge} = \frac{\|f_{eq}^z\|_\infty^k - \|f_{eq}^z\|_\infty^{k-1}}{\|f_{eq}^z\|_\infty^k} \tag{3.12}$$

is met in the outer loop, where the $\|f_{eq}^z\|_\infty^k$ term is the infinity norm of the equivalent static load vector for the current nonlinear evaluation and $\|f_{eq}^z\|_\infty^{k-1}$ is the infinity norm of equivalent static load vector for the previous nonlinear evaluation. This convergence tolerance is satisfied as shown in Fig. 3.5.

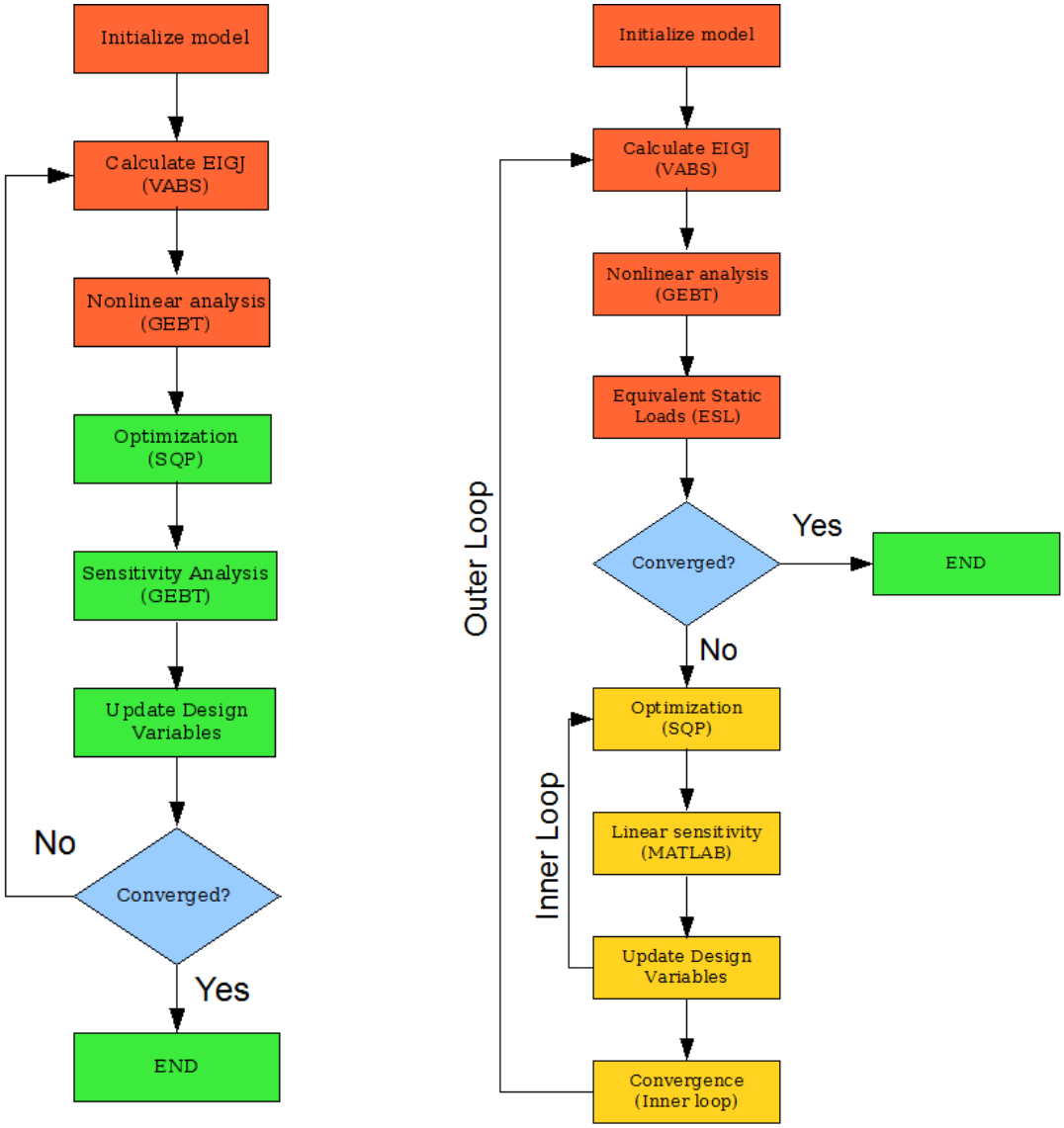

(a) GEBT (b) GEBT-ESL

Figure 3.5: Flow charts showing the difference between pure nonlinear optimization (GEBT) and nonlinear optimization with equivalent static loads (GEBT-ESL).

3.7 Limit Load Calculations

Initial efforts to perform the nonlinear optimization revealed peculiarities in the joined-wing optimization problem. In the first run attempted, the optimizer set all design variables to minimum gage after the first step in an attempt to minimize the weight of the structure. The problem arises that, when the minimum gage design as defined in this research is sent to GEBT for a nonlinear response analysis, the analysis fails. The issue is hinted at in a message returned by Mathematica, stating that the Jacobian used in the calculation of the solution is singular, and that the design should be adjusted in an effort to obtain a well behaved Jacobian. After failing to harness a flag from this error message as a means of triggering a 'bad design' indicator in MATLAB, an alternative approach is presented.

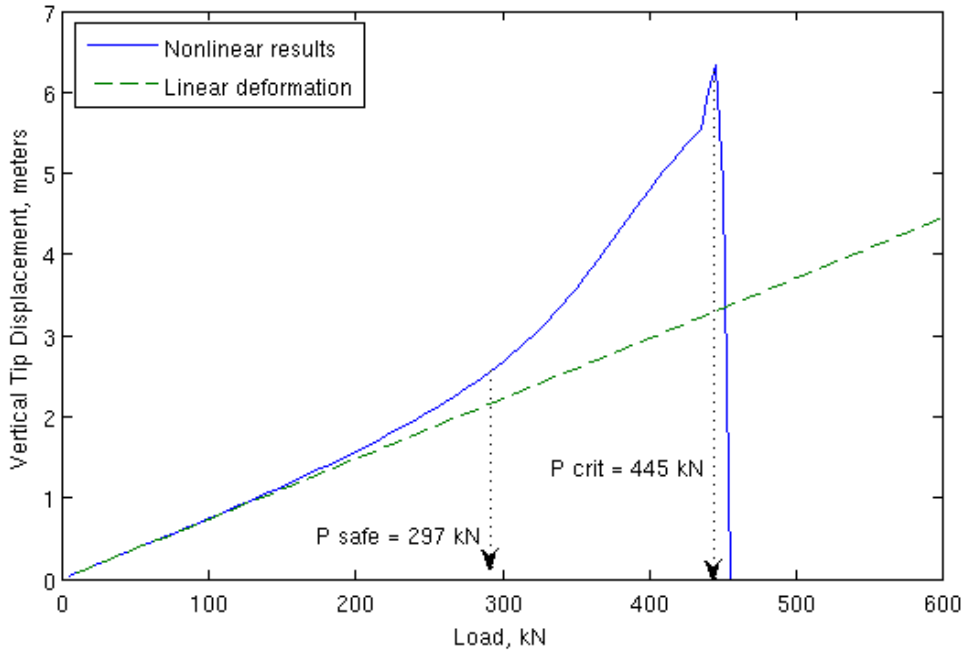

Figure 3.6: Load-deflection curve showing linear and nonlinear behavior. $P_{critical}$ is located at the peak of the nonlinear curve and indicates failure of the design.

Elasticity theory describes the load-deformation curve and uses it to show linear-elastic and nonlinear-elastic regions of deformation. If the load on a specimen continues to increase beyond the yield stress, behavior of the material cannot be predicted with GEBT. The analysis by GEBT shows this failure in the form of the poorly conditioned

stiffness matrix. The stiffness matrix becomes poorly conditioned due to the geometric nonlinearity effects. Geometric nonlinearities con manifest themselves either in an unstable stiffness matrix due to buckling (cannot be inverted) or by the presence of large nonlinear strain terms which render the stiffness matrix numerically ill conditioned (results unreliable). The solution to determining this failure criterion is to generate the load-deformation curve each time the constraints are evaluated to find the value of a $P_{critical}$ that is defined as the point where the deflection returned from the nonlinear solver is less than the previous value on the curve. A graphical example of this location is provided in Fig.3.6 where the nonlinear curve is at a maximum value of approximately 6.3 m. Furthermore, it is clear that operating near this region of the curve could be disastrous in a real world design, so a safety factor P_{safe} is defined

$$P_{safe} = \frac{P_{critical}}{1.5} \tag{3.13}$$

and used as a constraint on the optimization problem as

$$P_{applied} < P_{safe}. \tag{3.14}$$

It is possible to calculate a nonlinear optimization of this problem with less computational effort. Using rounded off values of the design variables, a comparison can be made that eliminates a large percentage of the nonlinear analysis overhead. For example, the following set of design variables are handed to the optimizer for step k_n:

$$\begin{aligned} c &= 1.2573874 \\ h &= 0.1088356 \\ t_s &= 0.0623400 \\ t_w &= 0.0500000 \end{aligned} \tag{3.15}$$

and are rounded off to four decimal places. The rounded off values for step k_n are

$$\begin{aligned} c &= 1.2574 \\ h &= 0.1088 \\ t_s &= 0.0623 \\ t_w &= 0.0500 \end{aligned} \tag{3.16}$$

which are stored for comparison during the next step in the optimization. During a finite difference method, the small value added to the design variables is on the order of 10^{-6} or smaller. In this example, 10^{-6} is used, so that the design variables for the next iteration k_{n+1} are

$$\begin{aligned} c &= 1.2573884 \\ h &= 0.1088366 \\ t_s &= 0.0623410 \\ t_w &= 0.0500010 \end{aligned} \tag{3.17}$$

which rounded off to four decimal places are the same values shown in Eqs. (3.17). When a comparison is made between the rounded set of design variables for step k_n and k_{n+1} they are found to be equivalent regarding the change in the shape of the load-displacement curve. There is still sufficient change when using the unrounded design variables to calculate the required displacement and stress sensitivities needed for SQP to choose the appropriate search direction. Now that the load-deflection curve is not changing with the finite difference calculations, it is then extended to the calculation of the critical and safe loads for a given design. Since the results for $P_{critical}$ and P_{safe} do not change after the first finite difference calculation, these nonlinear analyses do not need to be performed and can be removed while using the previous values for $P_{critical}$ and P_{safe} in a constraint.

Upon further investigation, it is clear that knowing the actual limit load is unnecessary if the design is safe. This is because the direction of search taken in the optimizer

will not be based on a constraint violation of the limit load. It is enough to know that P_{safe} is not less than the applied load. With this in mind, further time savings can be had by limiting the upper limit of the load-deformation curve calculation to no more than 1.5 times the applied tip load and implementing an active set strategy for the gradient calculation. This will ensure adequate determination of the constraint violations while removing all extraneous nonlinear calls in a nonlinear response optimization.

3.8 Limit Load Estimation Techniques

3.8.1 Polynomial Curve Fit with Equivalent Static Loads at Limit Load. In order to make a fair assessment in the gains offered by the use of ESL a means of including the limit load in the GEBT-ESL inner loop is desired. Also, inclusion of the limit load constraint should also guarantee that the limit load will not be violated by the final design returned from the optimizer. A second order polynomial curve fit is an important piece to an inner loop approximation of the limit load that can be applied as a constraint. Instead of defining the limit load curve with a constant step size, a selection of four to five points in the vicinity of the applied load and desired limit load are evaluated using GEBT. These loads then return a displacement vector for the loads under consideration. The use of a quadratic curve fit algorithm will result in the polynomial

$$P(u) = a_0 + a_1 u + a_2 u^2 \tag{3.18}$$

where a_0, a_1, and a_2 are the coefficients when the curve fit algorithm is supplied with the calculated displacements. This means Eq. (3.18) will return a load when supplied with a new displacement. To determine the displacement in the inner loop, a separate set of ESL are calculated in the outer loop for the limit load calculation using the maximum load used in the calculation of the curve fit data points in GEBT to return the true nonlinear wing tip displacement. Differentiating Eq. (3.18) with respect to tip displacement,

$$\frac{dP(u)}{du} = a_1 + 2 * a_2 u \tag{3.19}$$

which if set equal to zero can be solved for u_{limit}. Then using this new value for u_{limit} in Eq. (3.18) will produce an estimate of P_{limit} as shown in Fig. 3.7. Using u_{limit} an ESL can be calculated for the limit load displacement. Within the inner loop, the ESL at the limit load will generate different deflections at the limit load as the design variables are updated. Results with this P_{limit} estimation technique within the GEBT-ESL displacement constraint problem are shown in Table 4.4

The use of this method of P_{limit} estimation does yield some improvements over the calculation where P_{limit} is ignored as a constraint. In stiffer structures, the constraint appears to allow for a more efficient design, but at the cost of additional computational cost as shown in Table 4.4. This tradeoff of computational effort for much improved reliability is considered worth the investment. By comparing Fig. 4.1 to Fig. 4.2 it is clear there is improvement in the optimized mass of the structure when the wing tip deflection is constrained to 0.25 and 0.35 m. At the other end of the scale, use of the limit load estimation led to results at displacement constraint values that were previously unattainable for the 32-DV and 64-DV problems.

3.8.2 Polynomial Curve Fit with Updated Slope Term. Another possible approach to the estimation of P_{limit} is to update the a_1 or slope term in Eq. (3.18) inside the inner loop. The setup is the same in the outer loop as described in the previous section. When the polynomial is handed to the inner loop, a different calculation is performed. A ratio

$$\tilde{a}_1 = \frac{\tilde{u}_{applied}}{u_{applied}} a_1 \tag{3.20}$$

where $u_{applied}$ is the tip deflection calculated by GEBT in the outer loop at the applied load, a_1 is the coefficient of the polynomial calculated in the outer loop, $\tilde{u}_{applied}$ is the inner loop wing tip deflection estimated using ESL at the applied load, and $\tilde{a}_1$ is the updated value for the slope in the inner loop. The change in slope allows an update to the limit load in the linear analysis. This update method yields results similar to those provided in the previous section with no obvious advantage at this time.

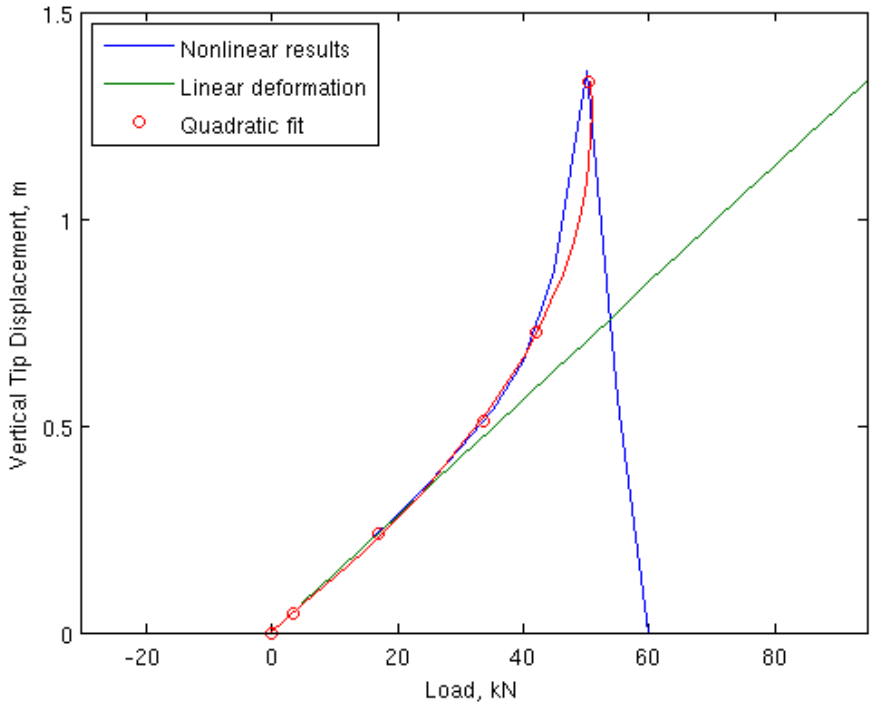

Figure 3.7: Plot showing the nonlinear load deflection curve using the incremental step method (blue solid line), the linear load deflection curve (green solid line), and the 2^{nd} order polynomial curve fit for the limit load using a sampling of 5 points.

3.9 Trust Region Strategy

Move limits play a vital role in the ability of the nonlinear response optimization to converge. The fixed reduction of the move limit does not always allow the overall MATLAB routine to converge to a solution that improved upon the 4-DV case when starting with the same initial design variables, even though SQP successfully converged in the inner optimization loop. Dynamic move limits can be used to allow the optimization routine to adjust the step size while searching for the optimal solution, but require additional information to work properly. A definition of when to expand, contract, or keep the current move limits is needed. Introduction of a trust region strategy proved to be an acceptable solution where the trust ratio ϕ is defined as

$$\phi = \frac{\psi_{k-1} - \psi_k}{\psi_{k-1} - \tilde{\psi}_k} \tag{3.21}$$

where ψ_{k-1} is the value of merit function based on the nonlinear analysis before the optimization loop, ψ_k is the value of the merit function based on the nonlinear analysis after the optimization loop, and $\tilde{\psi}_k$ is the value of the merit function using the equivalent static loads. The merit function used in the displacement constraint problem was defined as

$$\psi = \sqrt{(u_{tip} - u_{tip\ allow})^2} \tag{3.22}$$

where u_{tip} is the vertical displacement of the wing tip node and $u_{tip\ allow}$ is the allowed displacement of the same node. The trust region strategy allows the outer loop of the optimization to dynamically choose whether to maintain, expand, or contract the allowable move limits for the inner loop ESL optimization based on the value of ϕ after each result from the inner loop is returned. If a set of design variables are rejected, the values used to enter the inner optimization loop are restored and optimized again with contracted move limits. If ϕ indicates an improvement in the design, the move limits are kept the same. If ϕ shows a great improvement in the design, then the move limits are expanded in an attempt to allow the design to reach the optimum more quickly.

IV. Results and Discussion

THE results for the nonlinear optimization problem are presented here. Wing box shape and sizing is accomplished using the methods described in Chapter 3 and integration of GEBT and ESL is an effective combination to reduce computational effort while maintaining accuracy in the final solution. There are also some benefits to increasing the number of beam elements in the structure, at the expense of increasing the computational expense compared to smaller numbers of beam elements/degrees of freedom. Finally, although there is no mention in the literature regarding limit load criteria or constraints, it is shown here to be an important safety consideration which must be accounted for in the design optimization process.

4.1 Four Design Variables - Displacement Constraints

4.1.1 Nonlinear Optimization (GEBT). The full nonlinear response optimization solution with $u_{zallow} = 0.25$ m is shown in Table 4.1. The mass of the optimized structure is 1183.1 kg. Note that the results for all elements are the same due to the design variable linking in the 4-DV case. The results presented in Table 4.1 are the same when the limit load is calculated every time the constraints are evaluated and takes 4 hours 24 minutes to complete. Eliminating unneccessary calculation of the full load-deflection curve from the finite differencing calls using the rounded design variable comparison resulted in a run time of 33 minutes 34 seconds, a 92% time savings over the full analysis. A comparison of different approaches to the 4-DV dispacment constraint optimization problem is shown in Table 4.2.

Computationally, the addition of the limit load constraint is significant. The limit load for the initial set of design variables is more than 250,000 N, which requires 50 calls to the nonlinear solver with a step size of 5,000 N to determine this value. Other step sizes will change the required number of calls, but as P_{safe} approaches the applied load, a finer step size may be required to accurately determine if the design meets the limit load constraint. Computing the limit load calculation for every step in the finite differencing routine dramatically increases the time required to perform the optimization, on the order of hours instead of minutes or seconds.

Table 4.1: Solution to 4-DV displacement constraint nonlinear response optimization where $u_{zallow} = 0.25$ m

Element	c (m)	h (m)	t_{skin} (m)	t_{web} (m)
1	1.3339	0.2005	0.0050	0.0050
2	1.3339	0.2005	0.0050	0.0050
3	1.3339	0.2005	0.0050	0.0050
4	1.3339	0.2005	0.0050	0.0050
5	1.3339	0.2005	0.0050	0.0050
6	1.3339	0.2005	0.0050	0.0050
7	1.3339	0.2005	0.0050	0.0050
8	1.3339	0.2005	0.0050	0.0050

4.1.2 Nonlinear Optimization with Linear Approximation (GEBT-ESL). When equivalent static loads are introduced, they replace the full nonlinear analysis inside SQP with a linear approximation. This means inside the inner loop, there is no difficulty with a cumbersome constraint evaluation. As a result of using ESL and not requiring a limit load constraint, the time savings is three orders of magnitude between the full nonlinear GEBT and the GEBT-ESL solutions. It should be noted that the optimization for GBT-ESL did not evaluate the limit load constraint in any way. This frees GEBT-ESL from the computational effort required for nonlinear optimization that is largely due to calculating this constraint. Also, it is shown in Table 4.1 and Table 4.2 that the final solutions for each method return the same objective function value, P_{safe}, and design variable values. The only changes are in computational effort and time required. Note that the values for P_{safe} shown are calculated after the optimization is complete using the final design variable vector $\boldsymbol{b}$ and is not included in the time required to arrive at the solution. The results for the 4-DV displacement constraint problem using GEBT-ESL without limit load calculations are shown in Table 4.3 and Fig. 4.1.

4.2 Thirty-two Design Variables - Displacement Constraints

4.2.1 Move Limits and Move Reduction. Increasing the number of design variables for the displacement constraint scenario is studied. In this case, eight elements with four design variables each are all independent of each other for a total of thirty-two design variables (32-DV). Initially, it was believed that the code would be identical to that

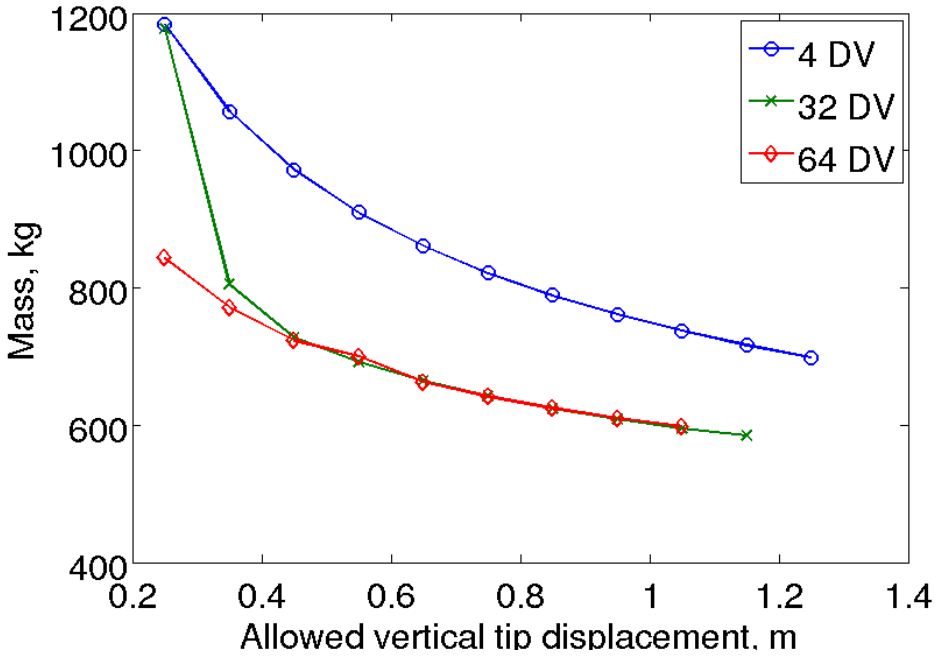

Figure 4.1: Pareto curve showing change in optimized mass as the tip deflection constraint is varied for 4, 32, and 64-DV cases

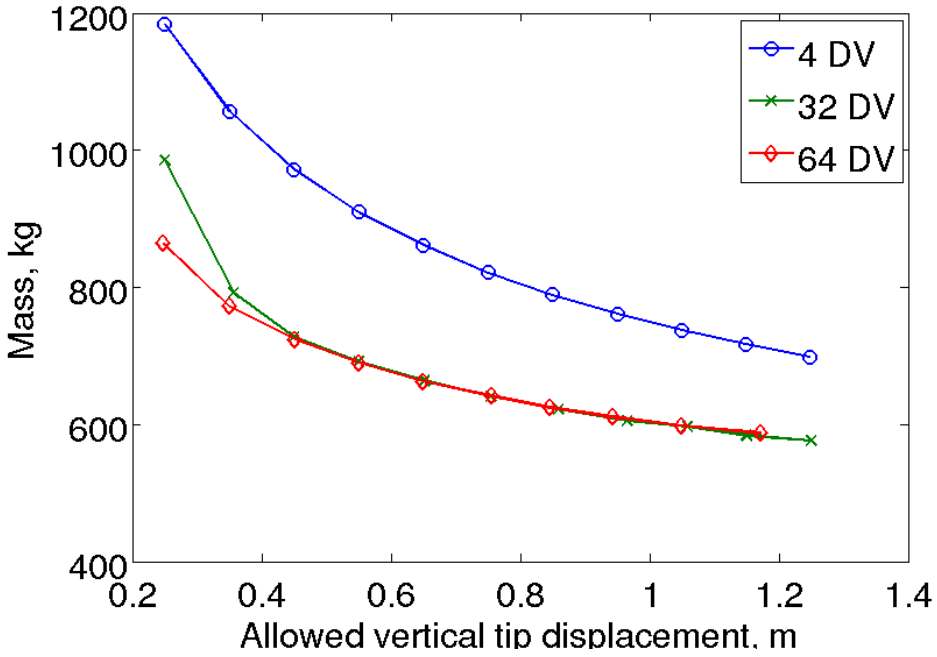

Figure 4.2: Pareto curve showing change in optimized mass as the tip deflection constraint is varied for 4, 32, and 64-DV cases with a 2^{nd} order polynomial curve fit estimate of P_{limit} applied as a constraint in the inner loop.

Table 4.2: Comparison of different solution techniques when applied to the four design variable optimization problem with a displacement constraint.

Solution Method	u_{zallow} (m)	f_{obj} (kg)	Move Limit	Move Reduction	Time Required	Nonlinear Calls	P_{safe} (kN)
GEBT	0.25	1183.1	0.09	0.7	4 h 23 m	>10,000	297
GEBT-DV compare	0.25	1183.1	0.09	0.7	33 m 34 s	1821	297
GEBT-DV compare with 2 x Load check	0.25	1183.1	0.09	0.7	8 40 s	304	297
GEBT-ESL	0.25	1183.1	0.09	0.7	8 s	4	297

of the 4-DV problem with independent values for c, h, t_s, and t_w. When an optimization is performed without move limits or use of the limit load calculation described in Section 3.7, the design shown in Table 4.5 is returned, with $f_{obj} = 861.6$ kg and $P_{safe} = 20$ kN. Time required for the analysis is 1 minutes 43 seconds, which is reasonable considering the increased number of design variables over the 4-DV case. The critical issue here is the violation of P_{safe} when checked at the end of the optimization. The advantage in computational time seen in the 4-DV case in GEBT-ESL disappears with the increase in the number of design variables.

Different approaches could potentially solve this issue, however caution must be exercised in selecting the method lest the advantages gained in using the equivalent static loads will disappear. Most obviously, the use of the limit load calculation originally described in the 4-DV nonlinear analysis could be used. It is still very costly, however, to calculate the load-deformation curve for each step of the optimization. This approach is not recommended as a result. A second possibility is the use of a trust region strategy in the outer loop of the ESL routine that will detect a violation of the limit load constraint and reduce the allowable change in design variables for a given nonlinear analysis. The reduction of the move limit continues until either the next step does not violate the limit load or the solution has converged. A third option is that move limits could be prescribed for each individual design variable, or made relative to each design variable as opposed to using absolute move limits for all DVs. If using relative move limits and the initial value of c is 1.5 m, while t_s is 0.015 m, it may be desirable to allow the value of c to vary $\pm$ 0.1 m while t_s is only allowed to vary $\pm$ 0.001 m per iteration. This technique becomes more important the larger the difference in magnitude of the design variables

Table 4.3: Optimization results for beam elements with displacement constraints.

Solution Method	$u_{z-allow}$ (m)	f_{obj} (kg)	Move Limit	Move Reduction	Time Required	Nonlinear Calls	P_{safe} (kN)
4-DV GEBT-ESL	0.25	1183.1	0.1	0.5	12 s	4	297
	0.35	1057.1	0.1	0.5	9 s	4	207
	0.45	972.3	0.1	0.5	10 s	5	160
	0.55	909.8	0.1	0.5	12 s	6	127
	0.65	861.1	0.1	0.5	12 s	6	107
	0.75	821.7	0.1	0.5	13 s	7	93
	0.85	789.0	0.1	0.5	14 s	7	80
	0.95	761.3	0.1	0.5	14 s	7	73
	1.05	737.5	0.1	0.5	14 s	7	70
	1.15	716.7	0.1	0.5	17 s	7	63
	1.25	698.4	0.1	0.5	19 s	9	57
32-DV GEBT-ESL	0.25	1177.8	0.09	0.7	55 s	11	120
	0.35	804.9	0.09	0.7	77 s	14	127
	0.45	727.7	0.10	0.5	30 s	7	97
	0.55	691.6	0.09	0.7	58 s	11	80
	0.65	664.4	0.10	0.5	73 s	18	77
	0.75	642.0	0.08	0.5	30 s	7	60
	0.85	623.7	0.09	0.7	40 s	8	53
	0.95	608.6	0.10	0.5	25 s	7	47
	1.05	595.2	0.09	0.7	38 s	8	43
	1.15	584.3	0.10	0.5	58 s	11	40
	1.25	-	-	-	-	-	-
64-DV GEBT-ESL	0.25	843.6	0.07	0.5	210 s	6	147
	0.35	771.6	0.07	0.5	162 s	6	107
	0.45	723.5	0.07	0.5	124 s	6	87
	0.55	700.4	0.07	0.5	254 s	8	60
	0.65	663.1	0.07	0.5	164 s	7	53
	0.75	641.9	0.07	0.7	161 s	7	47
	0.85	625.0	0.08	0.5	265 s	10	40
	0.95	610.4	0.08	0.5	143 s	7	40
	1.05	598.5	0.09	0.7	141 s	7	36

Table 4.4: Optimization results for beam elements with displacement constraints and $\boldsymbol{P_{safe}}$ polynomial curve fit estimation routine incorporated

Solution Method	$\boldsymbol{u_{z-allow}}$ (m)	$\boldsymbol{f_{obj}}$ (kg)	Move Limit	Move Reduction	Time Required	Nonlinear Calls	$\boldsymbol{P_{safe}}$ (kN)
4-DV GEBT-ESL	0.25	1183.1	0.1	0.5	21 s	16	293
	0.35	1057.1	0.1	0.5	21 s	16	207
	0.45	972.3	0.1	0.5	21 s	16	157
	0.55	909.8	0.1	0.5	21 s	16	133
	0.65	861.1	0.1	0.5	21 s	16	110
	0.75	821.7	0.1	0.5	27 s	21	97
	0.85	789.0	0.1	0.5	27 s	21	87
	0.95	761.4	0.1	0.5	28 s	21	73
	1.05	737.5	0.1	0.5	27 s	21	67
	1.15	716.9	0.1	0.5	27 s	21	60
	1.25	698.4	0.1	0.5	27 s	21	53
32-DV GEBT-ESL	0.25	985.1	0.09	0.7	310 s	178	120
	0.35	792.6	0.09	0.7	194 s	126	127
	0.45	727.6	0.10	0.5	68 s	42	97
	0.55	691.7	0.09	0.7	58 s	35	80
	0.65	663.8	0.10	0.5	198 s	133	77
	0.75	640.9	0.08	0.5	207 s	133	60
	0.85	622.0	0.09	0.7	201 s	133	53
	0.95	606.0	0.10	0.5	243 s	133	47
	1.05	596.7	0.09	0.7	228 s	140	43
	1.15	584.0	0.10	0.5	198 s	109	40
	1.25	576.0	0.10	0.5	348 s	231	40
64-DV GEBT-ESL	0.25	864.0	0.9	0.7	869 s	91	47
	0.35	772.3	0.4	0.7	162 s	28	95
	0.45	723.8	0.4	0.7	183 s	28	69
	0.55	689.9	0.4	0.7	196 s	35	69
	0.65	663.0	0.5	0.5	223 s	42	59
	0.75	642.0	0.5	0.7	350 s	63	48
	0.85	624.9	0.5	0.5	172 s	35	45
	0.95	610.9	0.5	0.5	171 s	35	41
	1.05	598.0	0.5	0.5	231 s	49	37
	1.15	598.0	0.5	0.8	318 s	49	37

being considered, as it will allow slower changes to the design that will more likely keep the design in the feasible design space as iterations occur.

Using move limits while ignoring inner loop calculation or approximation of the limit load, GEBT-ESL returns designs that meet the $P_{critical}$ value but still violate the P_{safe} constraint.There are also other difficulties that arise. When using the initial design variable values in Table 3.1, and an outer loop move limit on all design variables of 0.15 m, the design shown in Table 4.6 is the result. Of greatest concern is the fact that neither the front or aft wing tapers smoothly from the root to the tip in the chord and height variables. Also, the objective function value f_{obj} = 1706.3 kg is approximately a 500 kg increase over the 4-DV solution already calculated, so this cannot be the true global minimum. The fixed move limits do not afford the optimization problem the time needed to converge to a true minimum solution. When the move limits were expanded to allow SQP to move the design more quickly, the final result did not meet the limit load constraint.

Experimentation with different starting design variables showed that it is possible to improve upon the 4-DV GEBT-ESL results. When the initial values for the optimization were set to the values obtained for the 4-DV solution, GEBT-ESL was able to improve upon the 4-DV result. For move limit = 0.1 m and move reduction = 70 %, f_{obj} = 1097.5 kg and had a P_{safe} = 37 kN. This is a valid design satisfying all constraints, even though no limit load calculations were being performed during the optimization. As a result, only 1 min 43 sec were required to converge to the solution.

Note the only issue in Table 4.7 is that the the value of h for element 1 (0.1340 m) is less than the value for element 2 (0.1780 m). This violates the smooth taper from root to tip sought after in the design. While not strictly necessary, intuition would indicate that a smooth taper would be the lightest design in both a displacement or stress constrained optimization problem.

Adjusting the move limit to 0.05 m and leaving the move reduction at 70% returns the best solution seen to this point. The design satisfies all constraints, has a smooth taper from root to tip in both wings, and does not require calculation of the limit load within the algorithm. The value of the objective function is f_{obj} = 1122.9 kg, P_{safe} = 40

Table 4.5: Design variables by element for 32-DV GEBT-ESL design with no move limits or limit load calculation.

Element	chord	height	skin	web
1	1.8943	0.2842	0.0050	0.0083
2	1.6624	0.2494	0.0050	0.0082
3	1.3128	0.1969	0.0050	0.0082
4	0.7047	0.1057	0.0050	0.0084
5	0.5000	0.0250	0.0050	0.0010
6	0.5000	0.0250	0.0050	0.0010
7	0.5000	0.0250	0.0050	0.0010
8	0.5000	0.0250	0.0050	0.0010

Table 4.6: Design variables by element for 32-DV GEBT-ESL design with move limit = 0.15 m and move reduction = 70 % with no limit load calculation. Initial design variables are those used in Table 3.1.

Element	chord	height	skin	web
1	1.3982	0.1332	0.0089	0.0177
2	1.4477	0.1487	0.0089	0.0145
3	1.0647	0.1439	0.0089	0.0136
4	0.8934	0.0899	0.0089	0.0090
5	0.8883	0.0888	0.0089	0.0089
6	0.9214	0.1136	0.0089	0.0113
7	1.0496	0.1493	0.0089	0.0114
8	0.9901	0.1485	0.0089	0.0121

Table 4.7: Design variables by element for GEBT-ESL design with move limit = 0.10 m and move reduction = 70 % with no limit load calculation. Initial design variables are the solution to the 4-DV 0.25 m tip displacement constraint optimization problem.

Element	chord	height	skin	web
1	1.7252	0.1340	0.0050	0.0113
2	1.1904	0.1780	0.0050	0.0077
3	0.8935	0.1340	0.0050	0.0062
4	0.8935	0.1340	0.0050	0.0058
5	0.8935	0.1340	0.0050	0.0058
6	1.0401	0.1534	0.0050	0.0073
7	1.3493	0.1942	0.0050	0.0088
8	1.4743	0.2151	0.0050	0.0087

kN, and time required is 1 min 22 sec. Initial design variables were the solution design variables to the 4-DV displacement constraint problem for 0.25 m. The use of another answer to begin this process is the only weak point of this algorithm.

When the trust region strategy described in Section 3.9 is properly implemented, the 32-DV problem results shown in Table 4.3 are obtained. In particular, for all but the first case where the tip displacement is constrained to 0.25 meters, the 32-DV results offer an average 28.7% reduction in mass compared to the 4-DV results while satisfying all constraints. The cost here is an average four times increase in time required to determine the final solution over the 4-DV problem. However, these increased times are all still only between 25 and 77 seconds total for the solution. This level of design variable refinement seems to offer the best compromise in the displacement constraint problems in terms of time required, value of the objective function, and the value of the limit load, P_{safe}.

4.3 Sixty-four Design Variables - Displacement Constraints

Refining the mesh to a total of 16 beam elements yields results consistent with those from the previous two cases as shown in Tables 4.3 and 4.4 and Figures 4.1 and 4.2. In general, the objective function value either decreases or is within 1% of the value of the eight element mesh. An increase in computational effort is present as the number of finite difference calculations is doubled. The time cost is approximately four times that of the eight element mesh with little improvement in overall design. The exception is the case with the tip displacement constraint set to 0.25 meters. It appears that the

larger, stiffer models (i.e. higher mass) with smaller allowed tip displacements may stand to lose more mass with a more refined mesh.

4.4 Four Design Variables - Stress Constraints

Optimization is performed using GEBT-ESL on an eight element model where the von Mises stress constraint for aluminum with a 1.5 times safety factor applied is 179 MPa. Cases with 4 and 32 independent design variables are considered. The least amount of computational effort is required for the 4-DV problem, while the 32-DV problem allowed refinement in the optimized structure. In particular, Table 4.8 shows for the 32-DV case that all but one element are within 10% of the applied nonlinear stress constraint. Also shown is that elements 5 and 8 actually exceed the allowed stress constraint by 5% and 2%, respectively. This discrepancy arises from the outer loop convergence criteria used in the problem. The convergence tolerance is defined in Eq. (3.12). This outer loop tolerance must be set to 10^{-2} to allow convergence. If set to a tighter tolerance, the optimizer may enter an endless loop where the convergence tolerance ϵ is never satisfied. With this relatively "loose" convergence criteria, differences between the approximate and actual calculated nonlinear stresses will show up in the second digit. Furthermore, it should be noted that all of the values presented in Table 4.8 are the largest von Mises stresses chosen from values at the four corners of the mid-point cross section. This method satisfies the goal of this research by showing that the constraints can be applied effectively. With further refinement of the approach, tighter tolerances and evaluation of the stresses at the nodes vice the mid point of the beam will yield even more accurate designs.

4.5 Thirty-two Design Variables - Stress Constraints

The solution to the 32-DV stress constraint problem required 7 nonlinear evaluations and 207 seconds to return the results shown in Table 4.8. This design is the most flexible one presented in research that is known to satisfy displacement, stress, and limit load constraints. Note the design has fully stressed members in elements 1 through 4 with a well behaved taper for both chord and height while skin thickness is minimum

Table 4.8: Optimization results for beam elements with stress constraints.

Solution Method	f_{obj} (kg)	P_{safe} (kN)	u_{tip} (m)	elem	c (m)	h (m)	t_s (m)	t_w (m)	σ_{vm} (MPa)
4-DV GEBT-ESL	908.6	127	0.5591	1	1.0164	0.1525	0.0050	0.0055	177
				2	1.0164	0.1525	0.0050	0.0055	121
				3	1.0164	0.1525	0.0050	0.0055	72
				4	1.0164	0.1525	0.0050	0.0055	33
				5	1.0164	0.1525	0.0050	0.0055	32
				6	1.0164	0.1525	0.0050	0.0055	76
				7	1.0164	0.1525	0.0050	0.0055	131
				8	1.0164	0.1525	0.0050	0.0055	179
32-DV GEBT-ESL	662.7	53	0.7771	1	1.3897	0.2085	0.0050	0.0071	179
				2	1.1894	0.1784	0.0050	0.0063	179
				3	0.8748	0.1312	0.0050	0.0085	180
				4	0.5003	0.0250	0.0050	0.0384	179
				5	0.5000	0.0250	0.0050	0.0050	57
				6	0.5000	0.0250	0.0050	0.0050	90
				7	0.5000	0.0250	0.0050	0.0050	95
				8	0.5000	0.0250	0.0050	0.0050	140

gage for all 8 elements. The interesting variable behavior is in the web thickness for elements 3 and 4. The skin thickness in element 3 is larger that elements 1 and 2, although only by roughly 20 - 40%. Element 4, on the other hand, is roughly 5 to 7 times larger than the thicknesses inboard of it. From an aerodynamic point of view, this is the easiest place to have a non-tapering dimension without impact to external planform and profile.

Geometric bend/twist coupling is evident in Fig. 4.3. Both wings have a discontinuity at the 3/4 span point, but inboard of that point both wings appear to be fairly smooth in their nodal rotations. Considering all nodes except for the wing tip for the aft wing shows the geometric nonlinearity that drives the need for GEBT as the nonlinear solver. The twist in the aft wing approaches 1 degree of twist at 1/4 span before reversing to more than -4 degrees of twist at the 3/4 span node. This change in sign as well as the magnitude of the twist indicates the wing is undergoing considerable deformation apart from the calculated tip deflection of 0.7771 m. In fact, the inboard half of the aft wing will be experiencing a positive increase in angle of attack while the outborad section of the aft wing experiences over 4 degrees less angle of attack. This disparity in loading conditions could lead to flutter or failure when aerodynamic forces are considered.

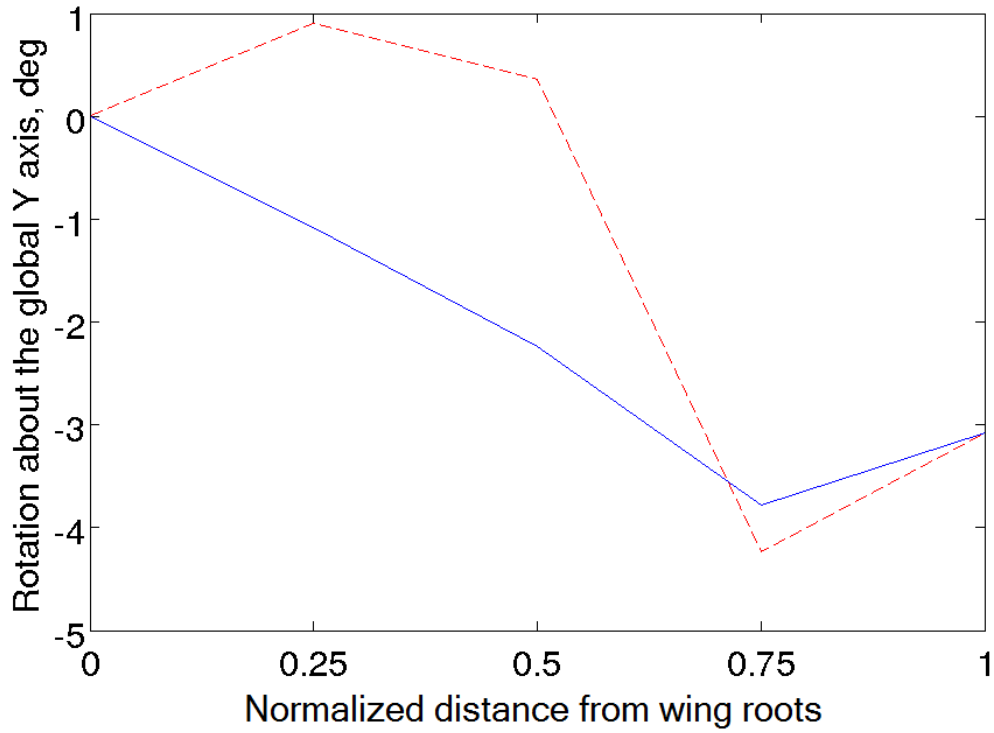

Figure 4.3: Plot taken from 32-DV stress constraint optimization showing twist in fore (blue solid line) and aft (red dashed line) wings as a function of normalized distance from the wing root.

Within the stress constraint optimization problem von Mises stresses are calculated for 32 different points in an 8 element structure. Each element compares the maximum von Mises stress present to the stress constraint defined in Eq. (3.10). The calculation of the von Mises stress produces a vector of nonlinear to linear stress ratios $\boldsymbol{\alpha}$ defined in Eq. (2.10). As the optimization process returns to the outer loop to update the nonlinear analysis, a new $\boldsymbol{\alpha}$ is calculalted. Instead of converging to unity, $\boldsymbol{\alpha}$ does not converge to anything meaningful. The stresses and stress ratio from the initial design and the final design for the 32-DV stress constraint problem is shown in Table 4.9.

It is possible that the random nature of the values for $\boldsymbol{\alpha}$ in Table 4.9 is a function of using the displacement based equivalent static loads and the stress ratio as described by MSC in their implementation of ESL [35]. It is unknown at this time if using the stress equivalent static loads described by Lee, et al. will produce a different result [5].

Table 4.9: Stress ratio results for 32-DV stress constraint problem

Element	First Iteration				Final Design			
	σ_{NL-VM} (MPa)	σ_{L-VM} (MPa)	α	σ'_{L-VM} (MPa)	σ_{NL-VM} (MPa)	σ_{L-VM} (MPa)	α	σ'_{L-VM} (MPa)
1	31.2	31.2	1.00	31.2	177.0	179.0	0.99	177.0
	21.8	19.8	1.10	21.8	105.0	99.2	1.06	105.0
	33.2	32.9	1.01	33.2	179.0	175.0	1.03	179.0
	20.0	21.6	0.93	20.0	94.1	94.8	0.99	94.1
2	21.4	22.2	0.96	21.4	176.0	216.0	0.82	176.0
	16.6	15.5	1.07	16.6	109.0	141.0	0.78	109.0
	23.4	22.1	1.06	23.4	179.0	138.0	1.30	179.0
	15.1	15.4	0.98	15.1	97.7	62.8	1.56	97.7
3	11.9	13.4	0.89	11.9	175.0	315.0	0.56	175.0
	11.1	10.9	1.02	11.1	111.0	240.0	0.46	111.0
	13.9	11.6	1.20	13.9	180.0	39.6	4.54	180.0
	10.0	9.1	1.11	10.0	96.7	37.5	2.58	96.7
4	3.8	4.2	0.90	3.8	179.0	774.0	0.23	179.0
	5.7	5.5	1.03	5.7	150.0	729.0	0.21	150.0
	5.3	2.0	2.73	5.3	174.0	382.0	0.45	174.0
	5.7	3.2	1.80	5.7	134.0	427.0	0.31	134.0
5	5.7	7.8	0.73	5.7	20.6	189.0	0.11	20.6
	3.6	6.2	0.58	3.6	38.4	243.0	0.16	38.4
	5.7	1.9	3.00	5.7	44.1	170.0	0.26	44.1
	4.9	1.7	2.85	4.9	56.8	115.0	0.49	56.8
6	10.9	12.9	0.85	10.9	89.5	138.0	0.65	89.5
	12.1	15.8	0.76	12.1	18.4	104.0	0.18	18.4
	9.9	6.8	1.45	9.9	49.8	50.2	0.99	49.8
	14.1	9.7	1.45	14.1	60.0	83.6	0.72	60.0
7	16.3	17.4	0.94	16.3	94.5	330.0	0.29	94.5
	21.6	24.6	0.88	21.6	57.5	318.0	0.18	57.5
	15.0	13.2	1.14	15.0	68.6	179.0	0.38	68.6
	23.8	20.4	1.17	23.8	79.9	191.0	0.42	79.9
8	22.0	22.2	0.99	22.0	78.3	152.0	0.52	78.3
	31.0	33.1	0.94	31.0	106.0	206.0	0.51	106.0
	20.6	19.8	1.04	20.6	55.4	23.5	2.35	55.4
	33.3	30.8	1.08	33.3	140.0	30.7	4.56	140.0

4.6 Failure to Converge to Displacement Constraint

There exist some combinations of move limits, move reductions, and allowable tip deflection that produce results that do not converge according to Eq. (3.12). An example of this is shown in Fig. 4.4. Due to the nonlinearity of the joined-wing problem, it is possible for the linear solution to converge within the inner loop after making changes in design variables that have greater sensitivity than the linear anlaysis is able to capture, even if a trust region strategy is employed. As a result, the ensuing outer loop nonlinear analysis with GEBT provides a tip displacement that is significantly different than the value at the end of the inner loop optimization. The disconnect then comes with the reduction in move limits before the next inner loop begins. When the step size is too small, the inner loop will not be able to move away from the "bad" set of design variables enough to get out of the region in the design space where the nonlinear analysis is so sensitive. A possible solution could be to apply the displacement constraint as a specific criterion in the trust region strategy in conjunction with the merit function shown in Eqs. (3.21) and (3.22).

4.7 Convergence from Outside the Limit Load Feasible Design Space

After applying the limit load approximation technique described in Section 3.8.2, a test was designed to determine how well the approximation technique dealt with a design that fails the limit load test. The chosen design was the lower limit, or minimum gage, for all design variables as shown in Eq. (3.10) in a 32-DV displacement constraint problem. The allowable tip deflection, u_{zallow}, was 0.70 m.

The first issue that arose was the trust region strategy described in Section 3.9 worked as desired. This meant that even though the linear response optimization attempted to increase the size of the design variables to produce a more robust structure, the trust region strategy negated these attempts due to a failure on the part of the new solution to improve upon the mass of the structure. Since the design is at a minimum possible mass of 398.94 kg when all design variables are minimum gage, the TR strategy believes it has the best solution available, regardless of the optmimzers efforts to achieve a feasible design.

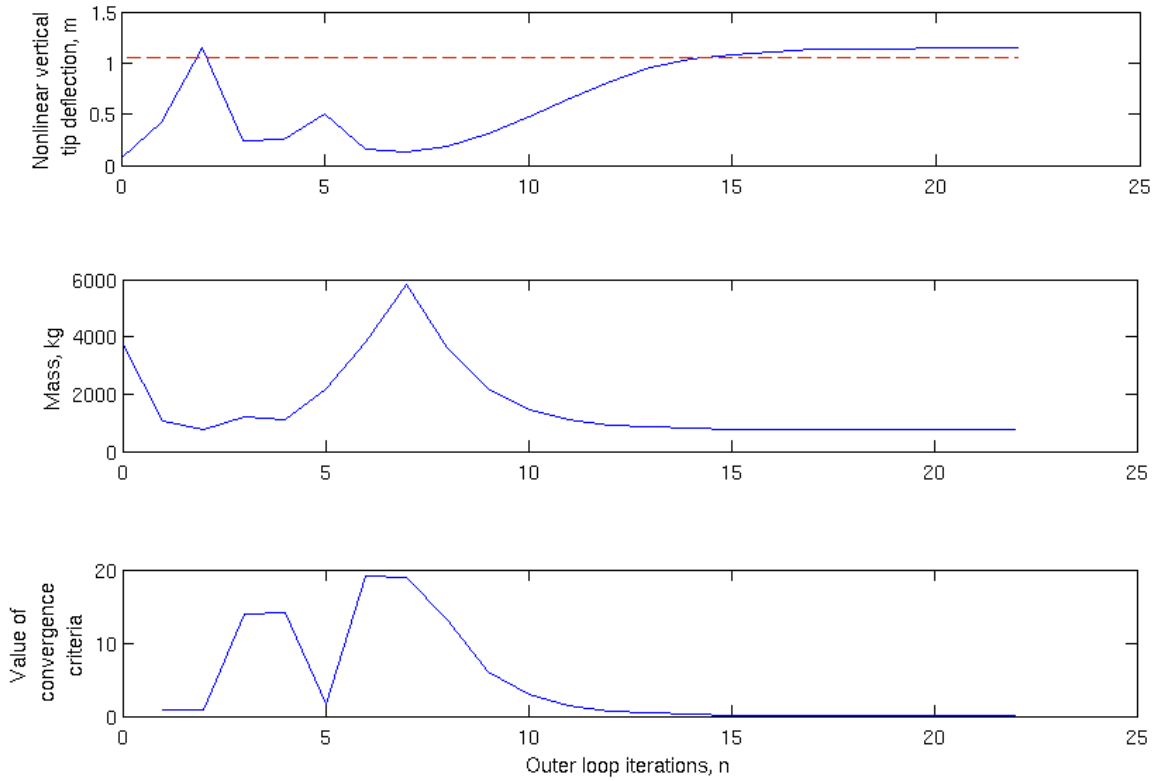

Figure 4.4: Three plots showing behavior of 32-DV nonlinear wing tip deflection attempting to converge to u_{tip} = 1.15 m, mass, and value of the the tolerance, Equation (3.12)

With the trust region strategy turned off, the optimizer was able to change the design variables in a manner that increased the stiffness and mass of the design. However, as stated previously, the convergence of this problem to a feasible design is still sensitive to the chosen move limits and move reduction ratio defined in the problem. Move limits of 0.5 and 1.5 applied to all design variables were too small and too large, respectively when paried with a 70% move reduction. However, when a move limit of 1.0 is combined with a 50% move reduction, the design shown in Table 4.10 is the result. This design is significant in that f_{obj} = 726.1 kg, and P_{safe} = 67 kN, a feasible design. It does not, however, lie on the Pareto curve for the 32-DV displacement problem shown in Fig. 4.2. The estimated value of f_{obj} is 652 kg for a displacement constraint problem where u_{zallow} = 0.70 m. The other interesting characteristic is that the optimizer chose a path that results in both wings tapering, instead of one going to minimum gage as is common

Table 4.10: Design variables by element for 32-DV GEBT-ESL design, $u_{allow} = 0.70$ m. Limit load estimated using ratio method described in Section 3.8.2.

Element	c (m)	h (m)	t_{skin} (m)	t_{web} (m)
1	1.0263	0.1539	0.0050	0.0050
2	0.8759	0.1211	0.0050	0.0050
3	0.6653	0.0879	0.0050	0.0050
4	0.5000	0.0607	0.0050	0.0050
5	0.5005	0.0751	0.0050	0.0050
6	0.7495	0.1124	0.0050	0.0050
7	1.0512	0.1577	0.0050	0.0050
8	1.2630	0.1783	0.0050	0.0050

when starting from the initial design variable values shown in Table 3.1. It is possible that more experimentation with move limits and move reduction ratio would produce an optimized design that lies on the Pareto front while remaining feasible with respect to the limit load and starting from an infeasible design. However, the larger issue lies with the incompatibillity of the trust region with the minimum gage initial design. Either a means of determining when to use the trust region needs to be defined, or all initial design variables should be chosen such that the initial design has greater mass than the anticipated final design.

V. Conclusions

5.1 Overview of Research Effort

A full nonlinear response optimization on the joined-wing design is presented. Design variables relating to the cross section of a simple box beam were sized using an SQP optimization routine. Geometrically exact beam theory is shown to be an effective tool in modeling the geometric nonlinearities exhibited by the joined-wing design. Further discretization of the fore and aft wings to a total of 16 elements with 64 design variables did not significantly improve on the optimized design in the displacement constraint problem. Considering this and the fact that the time required increased on average four times, it is clear that the 8 element, 32 design variable model offers the best compromise in time required and final optimized mass of the structure.

5.2 Conclusions

The use of equivalent static loads with GEBT are shown to be an effective solution method while offering significant savings in computational effort required. There exist unexplained sensitivities in the use of displacement based equivalent static loads that occasionally permit the optimization routine to converge to a displacement constraint in the nonlinear solution that is not the same as the applied constraint in the linear approximation. It is believed that these sensitivities are due at least in part to the move limit and move reduction allowed from iteration to iteration when a trust region strategy is applied. The current research has only applied the trust region strategy to the displacement constraint problem, so evaluation of the trust region effects do not apply to stress constraint problems at this time.

The need for consideration of additional constraints is shown. In particular, the limit load criterion and the requirement that the design remain feasible with respect to the limit load is a key safety consideration. While a finite difference approach to sensitivity analysis is used, the determination of this constraint is problematic. The easiest and computationally costliest approach is to recompute the load-deflection curve whenever a change is made to the design variables. This method renders the use of equivalent static loads ineffective due to the number of nonlinear calculations required to determine the

load-deflection curve for each iteration in the linear response optimization. An alternate means of determining the limit load using a second order polynomial approximation which updates the slope term during the linear FEM optimization was presented and shown to be effective.

5.3 Future Work

Future work should focus on determining the how the move limit and move reduction sizes affect the solution so that more general optimization problems can be set up with less interaction required on the part of the user. This will require a more detailed analysis of the logic employed in the trust region strategy currently employed. It is also planned that the trust ratio would be expanded to include stress constraint problems as well as displacement constraints.

Also, working to implement the stress based equivalent static loads (SBESL) described by Lee et al. [5] and making a comparison between SBESL and the results presented in this research would be beneficial. While MSC has opted for the simpler implementation shown here, it remains to be seen if there is an appreciable difference in results when using one method or the other. The expectation at this time is that α would reduce to unity when the optimizatino returns a final solution. If there is little to no difference between SBESL and the method used in this research, it begs the question of how important is the source data for the stress case as long as a stress ratio correction is applied.

A scale model of an optimized design made of aluminum box tubes is planned for laboratory experimentation to compare and contrast to the results obtained using the method outlined in this research. Tip loads and joint loads are planned on a design that locates the wing joint at less than 100% span of the forward wing.

Finally, incorporation of shape optimization of planform will allow a greater level of optimization based on aerodynamic, structural, and sensor effectiveness sensitivities. Consideration for this implementation must include the application of coordinate transformation from a change in angles in both sweep and dihedral for both wings. With these design variables included, a very complete and robust design analysis can be conducted

on airfoil shapes and orientation which should show the path to the most efficient design for the joined-wing Sensorcraft concept.

Appendix A. Optimization Results for 4-DV Optimization with Displacement Constraints

The following tables show the cross sectional dimensions of the final design obtained for 4, 32, and 64-DV problems with varying displacement constraints applied.

Table A.1: Design variables by element for 4-DV GEBT-ESL design, P-limit estimation used for limit load calculation.

u_{allow}	c (m)	h (m)	t_{skin} (m)	t_{web} (m)
0.25	1.3368	0.2005	0.0050	0.0050
0.35	1.1954	0.1793	0.0050	0.0050
0.45	1.0010	0.1650	0.0050	0.0050
0.55	1.0299	0.1545	0.0050	0.0050
0.65	0.9753	0.1463	0.0050	0.0050
0.75	0.9311	0.1397	0.0050	0.0050
0.85	0.8945	0.1342	0.0050	0.0050
0.95	0.8634	0.1295	0.0050	0.0050
1.05	0.8367	0.1255	0.0050	0.0050
1.15	0.8135	0.1220	0.0050	0.0050
1.25	0.7931	0.1190	0.0050	0.0050

Appendix B. Optimization Results for 32-DV Optimization with Displacement Constraints

The following tables show the cross sectional dimensions of the final design obtained for 4, 32, and 64-DV problems with varying displacement constraints applied.

Table B.1: Design variables by element for 32-DV GEBT-ESL design, $u_{allow} = 0.25$ m. No move limits or limit load calculation.

Element	c (m)	h (m)	t_{skin} (m)	t_{web} (m)
1	1.3969	0.1777	0.0050	0.0050
2	1.3969	0.1069	0.0050	0.0050
3	1.3969	0.0719	0.0050	0.0050
4	1.3969	0.0719	0.0050	0.0050
5	1.3969	0.0719	0.0050	0.0050
6	1.3969	0.1063	0.0050	0.0050
7	1.3969	0.1759	0.0050	0.0050
8	1.4818	0.2218	0.0050	0.0050

Table B.2: Design variables by element for 32-DV GEBT-ESL design, $u_{allow} = 0.35$ m. No move limits or limit load calculation.

Element	c (m)	h (m)	t_{skin} (m)	t_{web} (m)
1	0.5775	0.0300	0.0050	0.0050
2	0.5775	0.0300	0.0050	0.0050
3	0.5775	0.0300	0.0050	0.0050
4	0.5775	0.0300	0.0050	0.0050
5	0.7161	0.1074	0.0050	0.0050
6	1.1824	0.1770	0.0050	0.0050
7	1.5100	0.2260	0.0050	0.0050
8	1.7775	0.2660	0.0050	0.0050

Table B.3: Design variables by element for 32-DV GEBT-ESL design, $u_{allow} = 0.45$ m. No move limits or limit load calculation.

Element	c (m)	h (m)	t_{skin} (m)	t_{web} (m)
1	0.5000	0.0250	0.0050	0.0050
2	0.5000	0.0250	0.0050	0.0050
3	0.5000	0.0250	0.0050	0.0050
4	0.5000	0.0250	0.0050	0.0050
5	0.6587	0.0985	0.0050	0.0050
6	1.0924	0.1639	0.0050	0.0050
7	1.3913	0.2087	0.0050	0.0050
8	1.6363	0.2449	0.0050	0.0050

Table B.4: Design variables by element for 32-DV GEBT-ESL design, $u_{allow} = 0.55$ m. No move limits or limit load calculation.

Element	c (m)	h (m)	t_{skin} (m)	t_{web} (m)
1	0.5000	0.0250	0.0050	0.0050
2	0.5000	0.0250	0.0050	0.0050
3	0.5000	0.0250	0.0050	0.0050
4	0.5000	0.0250	0.0050	0.0050
5	0.6192	0.0922	0.0050	0.0050
6	1.0186	0.1525	0.0050	0.0050
7	1.2963	0.1942	0.0050	0.0050
8	1.5238	0.2274	0.0050	0.0050

Table B.5: Design variables by element for 32-DV GEBT-ESL design, $u_{allow} = 0.65$ m. No move limits or limit load calculation.

Element	c (m)	h (m)	t_{skin} (m)	t_{web} (m)
1	0.5000	0.0250	0.0050	0.0050
2	0.5000	0.0250	0.0050	0.0050
3	0.5000	0.0250	0.0050	0.0050
4	0.5000	0.0250	0.0050	0.0050
5	0.5939	0.0888	0.0050	0.0050
6	0.9630	0.1442	0.0050	0.0050
7	1.2206	0.1828	0.0050	0.0050
8	1.4313	0.2145	0.0050	0.0051

Table B.6: Design variables by element for 32-DV GEBT-ESL design, $u_{allow} = 0.75$ m. No move limits or limit load calculation.

Element	c (m)	h (m)	t_{skin} (m)	t_{web} (m)
1	0.5000	0.0250	0.0050	0.0050
2	0.5000	0.0250	0.0050	0.0050
3	0.5000	0.0250	0.0050	0.0050
4	0.5000	0.0250	0.0050	0.0050
5	0.5634	0.0845	0.0050	0.0050
6	0.9197	0.1380	0.0050	0.0050
7	1.1670	0.1750	0.0050	0.0050
8	1.3583	0.2037	0.0050	0.0050

Table B.7: Design variables by element for 32-DV GEBT-ESL design, $u_{allow} = 0.85$ m. No move limits or limit load calculation.

Element	c (m)	h (m)	t_{skin} (m)	t_{web} (m)
1	0.5000	0.0250	0.0050	0.0050
2	0.5000	0.0250	0.0050	0.0050
3	0.5000	0.0250	0.0050	0.0050
4	0.5000	0.0250	0.0050	0.0050
5	0.5440	0.0816	0.0050	0.0050
6	0.8815	0.1322	0.0050	0.0050
7	1.1174	0.1676	0.0050	0.0050
8	1.3011	0.1952	0.0050	0.0050

Table B.8: Design variables by element for 32-DV GEBT-ESL design, $u_{allow} = 0.95$ m. No move limits or limit load calculation.

Element	c (m)	h (m)	t_{skin} (m)	t_{web} (m)
1	0.5000	0.0250	0.0050	0.0050
2	0.5000	0.0250	0.0050	0.0050
3	0.5000	0.0250	0.0050	0.0050
4	0.5000	0.0250	0.0050	0.0050
5	0.5355	0.0803	0.0050	0.0050
6	0.8484	0.1273	0.0050	0.0050
7	1.0696	0.1604	0.0050	0.0050
8	1.2549	0.1882	0.0050	0.0050

Table B.9: Design variables by element for 32-DV GEBT-ESL design, $u_{allow} = 1.05$ m. No move limits or limit load calculation.

Element	c (m)	h (m)	t_{skin} (m)	t_{web} (m)
1	0.5000	0.0250	0.0050	0.0050
2	0.5000	0.0250	0.0050	0.0050
3	0.5000	0.0250	0.0050	0.0050
4	0.5000	0.0250	0.0050	0.0050
5	0.5163	0.0774	0.0050	0.0050
6	0.8301	0.1245	0.0050	0.0050
7	1.0386	0.1558	0.0050	0.0050
8	1.2033	0.1805	0.0050	0.0050

Table B.10: Design variables by element for 32-DV GEBT-ESL design, $u_{allow} = 1.15$ m. No move limits or limit load calculation.

Element	c (m)	h (m)	t_{skin} (m)	t_{web} (m)
1	0.5000	0.0265	0.0050	0.0050
2	0.5000	0.0250	0.0050	0.0050
3	0.5000	0.0250	0.0050	0.0050
4	0.5000	0.0250	0.0050	0.0050
5	0.5119	0.0762	0.0050	0.0050
6	0.8113	0.1217	0.0050	0.0050
7	1.0017	0.1500	0.0050	0.0050
8	1.1669	0.1731	0.0050	0.0050

Table B.11: Design variables by element for 32-DV GEBT-ESL design, $u_{allow} = 1.25$ m. No move limits or limit load calculation.

Element	c (m)	h (m)	t_{skin} (m)	t_{web} (m)
1	0.8196	0.1220	0.0050	0.0050
2	0.6969	0.0957	0.0050	0.0050
3	0.6969	0.0394	0.0050	0.0050
4	0.6969	0.0349	0.0050	0.0050
5	0.6969	0.0375	0.0050	0.0050
6	0.7245	0.1087	0.0050	0.0050
7	0.8531	0.1231	0.0050	0.0050
8	0.9362	0.1356	0.0050	0.0050

Appendix C. Optimization Results for 64-DV Optimization with Displacement Constraints

The following tables show the cross sectional dimensions of the final design obtained for 64-DV problems with varying displacement constraints applied.

Table C.1: Design variables by element for 64-DV GEBT-ESL design, $u_{allow} = 0.25$ m. No move limits or limit load calculation.

Element	c (m)	h (m)	t_{skin} (m)	t_{web} (m)
1	0.5000	0.0288	0.0050	0.0050
2	0.5000	0.0250	0.0050	0.0050
3	0.5000	0.0250	0.0050	0.0050
4	0.5000	0.0250	0.0050	0.0050
5	0.5000	0.0250	0.0050	0.0050
6	0.5000	0.0250	0.0050	0.0050
7	0.5000	0.0250	0.0050	0.0050
8	0.5000	0.0250	0.0050	0.0050
9	0.5902	0.0885	0.0050	0.0050
10	0.9638	0.1446	0.0050	0.0050
11	1.2166	0.1825	0.0050	0.0050
12	1.4304	0.2146	0.0050	0.0050
13	1.6155	0.2423	0.0050	0.0050
14	1.7868	0.2680	0.0050	0.0050
15	1.9419	0.2910	0.0050	0.0050
16	2.0895	0.3134	0.0050	0.0050

Table C.2: Design variables by element for 64-DV GEBT-ESL design, $u_{allow} = 0.35$ m. No move limits or limit load calculation.

Element	c (m)	h (m)	t_{skin} (m)	t_{web} (m)
1	0.5000	0.0250	0.0050	0.0050
2	0.5000	0.0250	0.0050	0.0050
3	0.5000	0.0250	0.0050	0.0050
4	0.5000	0.0250	0.0050	0.0050
5	0.5000	0.0250	0.0050	0.0050
6	0.5000	0.0250	0.0050	0.0050
7	0.5000	0.0250	0.0050	0.0050
8	0.5000	0.0250	0.0050	0.0050
9	0.5198	0.0780	0.0050	0.0050
10	0.8544	0.1282	0.0050	0.0050
11	1.0881	0.1632	0.0050	0.0050
12	1.2801	0.1920	0.0050	0.0050
13	1.4434	0.2165	0.0050	0.0050
14	1.5896	0.2384	0.0050	0.0050
15	1.7251	0.2588	0.0050	0.0050
16	1.8452	0.2768	0.0050	0.0050

Table C.3: Design variables by element for 64-DV GEBT-ESL design, $u_{allow} = 0.45$ m. No move limits or limit load calculation.

Element	c (m)	h (m)	t_{skin} (m)	t_{web} (m)
1	0.5000	0.0250	0.0050	0.0050
2	0.5000	0.0250	0.0050	0.0050
3	0.5000	0.0250	0.0050	0.0050
4	0.5000	0.0250	0.0050	0.0050
5	0.5000	0.0250	0.0050	0.0050
6	0.5000	0.0250	0.0050	0.0050
7	0.5000	0.0250	0.0050	0.0050
8	0.5000	0.0250	0.0050	0.0050
9	0.5000	0.0750	0.0050	0.0050
10	0.7840	0.1176	0.0050	0.0050
11	0.9975	0.1496	0.0050	0.0050
12	1.1669	0.1750	0.0050	0.0050
13	1.3196	0.1979	0.0050	0.0050
14	1.4535	0.2180	0.0050	0.0050
15	1.5741	0.2361	0.0050	0.0050
16	1.6860	0.2529	0.0050	0.0050

Table C.4: Design variables by element for 64-DV GEBT-ESL design, $u_{allow} = 0.55$ m. No move limits or limit load calculation.

Element	c (m)	h (m)	t_{skin} (m)	t_{web} (m)
1	1.6297	0.2442	0.0050	0.0050
2	1.5151	0.2273	0.0050	0.0050
3	1.3929	0.2089	0.0050	0.0050
4	1.2607	0.1891	0.0050	0.0050
5	1.1120	0.1668	0.0050	0.0050
6	0.9427	0.1411	0.0050	0.0050
7	0.7385	0.1096	0.0050	0.0050
8	0.5000	0.0486	0.0050	0.0050
9	0.5000	0.0250	0.0050	0.0050
10	0.5000	0.0250	0.0050	0.0050
11	0.5000	0.0250	0.0050	0.0050
12	0.5000	0.0250	0.0050	0.0050
13	0.5000	0.0250	0.0050	0.0050
14	0.5000	0.0250	0.0050	0.0050
15	0.5000	0.0250	0.0050	0.0050
16	0.5000	0.0250	0.0050	0.0050

Table C.5: Design variables by element for 64-DV GEBT-ESL design, $u_{allow} = 0.65$ m. No move limits or limit load calculation.

Element	c (m)	h (m)	t_{skin} (m)	t_{web} (m)
1	0.5000	0.0250	0.0050	0.0050
2	0.5000	0.0250	0.0050	0.0050
3	0.5000	0.0250	0.0050	0.0050
4	0.5000	0.0250	0.0050	0.0050
5	0.5000	0.0250	0.0050	0.0050
6	0.5000	0.0250	0.0050	0.0050
7	0.5000	0.0250	0.0050	0.0050
8	0.5000	0.0250	0.0050	0.0050
9	0.5000	0.0597	0.0050	0.0050
10	0.7009	0.1046	0.0050	0.0050
11	0.8825	0.1324	0.0050	0.0050
12	1.0311	0.1547	0.0050	0.0050
13	1.1613	0.1742	0.0050	0.0050
14	1.2751	0.1912	0.0050	0.0050
15	1.3814	0.2065	0.0050	0.0050
16	1.4800	0.2205	0.0050	0.0050

Table C.6: Design variables by element for 64-DV GEBT-ESL design, $u_{allow} = 0.75$ m. No move limits or limit load calculation.

Element	c (m)	h (m)	t_{skin} (m)	t_{web} (m)
1	0.5000	0.0250	0.0050	0.0050
2	0.5000	0.0250	0.0050	0.0050
3	0.5000	0.0250	0.0050	0.0050
4	0.5000	0.0250	0.0050	0.0050
5	0.5000	0.0250	0.0050	0.0050
6	0.5000	0.0250	0.0050	0.0050
7	0.5000	0.0250	0.0050	0.0050
8	0.5000	0.0250	0.0050	0.0050
9	0.5000	0.0540	0.0050	0.0050
10	0.6756	0.1001	0.0050	0.0050
11	0.8425	0.1264	0.0050	0.0050
12	0.9842	0.1476	0.0050	0.0050
13	1.1056	0.1658	0.0050	0.0050
14	1.2123	0.1819	0.0050	0.0050
15	1.3162	0.1963	0.0050	0.0050
16	1.4012	0.2094	0.0050	0.0050

Table C.7: Design variables by element for 64-DV GEBT-ESL design, $u_{allow} = 0.85$ m. No move limits or limit load calculation.

Element	c (m)	h (m)	t_{skin} (m)	t_{web} (m)
1	0.5001	0.0250	0.0050	0.0050
2	0.5001	0.0250	0.0050	0.0050
3	0.5001	0.0250	0.0050	0.0050
4	0.5001	0.0250	0.0050	0.0050
5	0.5001	0.0250	0.0050	0.0050
6	0.5001	0.0250	0.0050	0.0050
7	0.5000	0.0250	0.0050	0.0050
8	0.5001	0.0250	0.0050	0.0050
9	0.5001	0.0494	0.0050	0.0050
10	0.6511	0.0970	0.0050	0.0050
11	0.8134	0.1220	0.0050	0.0050
12	0.9428	0.1414	0.0050	0.0050
13	1.0627	0.1594	0.0050	0.0050
14	1.1627	0.1744	0.0050	0.0050
15	1.2533	0.1878	0.0050	0.0050
16	1.3425	0.1999	0.0050	0.0050

Table C.8: Design variables by element for 64-DV GEBT-ESL design, $u_{allow} = 0.95$ m. No move limits or limit load calculation.

Element	c (m)	h (m)	t_{skin} (m)	t_{web} (m)
1	0.5000	0.0250	0.0050	0.0050
2	0.5000	0.0250	0.0050	0.0050
3	0.5000	0.0250	0.0050	0.0050
4	0.5000	0.0250	0.0050	0.0050
5	0.5000	0.0250	0.0050	0.0050
6	0.5000	0.0250	0.0050	0.0050
7	0.5000	0.0250	0.0050	0.0050
8	0.5000	0.0250	0.0050	0.0050
9	0.5000	0.0461	0.0050	0.0050
10	0.6349	0.0941	0.0050	0.0050
11	0.7871	0.1179	0.0050	0.0050
12	0.9142	0.1371	0.0050	0.0050
13	1.0235	0.1535	0.0050	0.0050
14	1.1191	0.1679	0.0050	0.0050
15	1.2077	0.1806	0.0050	0.0050
16	1.2923	0.1921	0.0050	0.0050

Table C.9: Design variables by element for 64-DV GEBT-ESL design, $u_{allow} = 1.05$ m. No move limits or limit load calculation.

Element	c (m)	h (m)	t_{skin} (m)	t_{web} (m)
1	0.5000	0.0250	0.0050	0.0050
2	0.5000	0.0250	0.0050	0.0050
3	0.5000	0.0250	0.0050	0.0050
4	0.5000	0.0250	0.0050	0.0050
5	0.5000	0.0250	0.0050	0.0050
6	0.5000	0.0250	0.0050	0.0050
7	0.5000	0.0250	0.0050	0.0050
8	0.5000	0.0250	0.0050	0.0050
9	0.5000	0.0424	0.0050	0.0050
10	0.6225	0.0934	0.0050	0.0050
11	0.7738	0.1161	0.0050	0.0050
12	0.8820	0.1323	0.0050	0.0050
13	0.9966	0.1495	0.0050	0.0050
14	1.0873	0.1631	0.0050	0.0050
15	1.1657	0.1749	0.0050	0.0050
16	1.2363	0.1854	0.0050	0.0050

Appendix D. Third Possible Limit Load Estimation Technique

THE discussion on limit loads and ways to estimate them in Sections 3.7 and 3.8.2 covered approaches used in this research. A potential third option exists which is based on the sensitivity of the limit loads with respect to the design variables. This is shown as

$$\tilde{P}_{lim} = P_{lim} + \nabla P_{lim}^{T} \Delta X \tag{D.1}$$

where $\tilde{P}_{lim}$ is the approximate limit load, P_{lim} is the limit load about which the sensitivities exist, ∇P_{lim}^{T} is the vector of partial derivatives of P_{lim} with respect to each design variable, and ΔX is the vector of change in the value of the design variables. Analytic sensitivities of the limit load could be easily used with the other information already available to provide a quick estimate of the limit load. Calculation of analytic sensitivities should be included in future work as a tool to further refine the optimization of the joined-wing beam model used in this research.

Bibliography

1. Bowers, P. M., *Unconventional Aircraft*, Tab Books, Inc., Blue Ridge Summit, PA, 1984.
2. Wolkovitch, J., "Joined Wing Aircraft," U.S. Patent 4,365,773, December 28, 1982.
3. Wolkovitch, J., "The Joined-Wing: An Overview," *Journal of Aircraft*, Vol. 23, No. 3, 1986, pp. 161–178.
4. Gallman, J. W. and Kroo, I. M. , "Structural Optimization of Joined-Wing Synthesis," *Journal of Aircraft*, Vol. 33, No. 1, 1996, pp. 214–223.
5. Lee, H., Kim, Y. I., and Park G. J., et al., "Structural Optimization of a Joined-Wing Using Equivalent Static Loads," *Journal of Aircraft*, Vol. 44, No. 4, 2007, pp. 1302–1308.
6. Kim, Y., Park, G. J., Kolonay, R., Blair, M., and Canfield, R. A., "Nonlinear Response Structural Optimization of a Joined-Wing Using Equivalent Static Loads," *AIAA Journal*, Vol. 46, No. 11, 2008, pp. 2703–2713.
7. Hodges, D. H., Atilgan, A., Cesnik, C. E. S., and Fulton, M., "On a Simplified Strain Energy Function for Geometrically Nonlinear Behavior of Aniostropic Beams," *Composites Engineering*, Vol. 2, 1992, pp. 513–526.
8. Cesnik, C. E. S. and Hodges, D. H., "VABS: A New Concept for Composite Rotor Blade Cross Sectional Modeling," *Journal of the American Helicopter Society*, Vol. 42, 1997, pp. 27–38.
9. Yu, W., Hodges, D. H., Volovoi, V. V., and Cesnik, C. E. S., "On Timoshenko-like Modeling of Initially Curved and Twisted Composite Beams," *International Journal of Solids and Structures*, Vol. 39, 2002, pp. 5101–5121.
10. Blair, M. and Stritz, A., "Finite Element Beam Assemblies with Geometric Bend-Twist Coupling," AIAA/ASME/ASCE/AHS/ASC Structures, Structural Dynamics, and Materials Conference, Schaumberg, IL, 2008.
11. Hodges, D. H., "A Mixed Variational Formulation Based on Exact Intrinsic Equations for Dynamics of Moving Beams," *International Journal of Solids and Structures*, Vol. 26, 1990, pp. 1253–1273.
12. Hodges, D. H., *Nonlinear Composite Beam Theory*, American Institute of Aeronautics and Astronautics, Inc., Reston, VA, 2006.
13. Kunz, D., "Survey and Comparison of Engineering Beam Theories for Helicopter Rotor Blades," *Journal of Aircraft*, Vol. 31, 1994, pp. 473–479.
14. Li, L., Volovoi, V. V., and Hodges, D. H., "Cross Setional Design of Composite Rotor Blades," *Journal of the American Helicopter Society*, Vol. 53, 2008, pp. 240–251.
15. Volovoi, V. V., Hodges, D. H., Cesnik, C. E. S., and Popescu, B., "Assessment of Beam Modeling Methods for Rotor Blade Applications," *Mathematical and Computer Modeling*, Vol. 33, 2001, pp. 1099–1112.

16. Johnson, W., "Rotorcraft Aerodynamics Models for a Comprehensive Analysis," Proceedings of the 54th Annual Forum of the American Helicopter Society, Washington, D.C., 1998.

17. Johnson, W., "Rotorcraft Dynamics Models for a Comprehensive Analysis," Proceedings of the 54th Annual Forum of the American Helicopter Society, Washington, D.C., 1998.

18. Bauchau, O., "Computational Schemes for Flexible, Nonlinear Multi-Body Systems," *Multibody System Dynamics*, Vol. 2, 1998, pp. 169–225.

19. Saberi, H. A., Khoshlahjeh, M., Ormiston, R. A., and Rutkowski, M. J., "RCAS Overview and Application to Advanced Rotorcraft Problems," 4th Decennial Specialists' Conference on Aeromechanics, American Helicopter Society, 21-23 Jan 2004.

20. Cesnik, C. E. S. and Brown, E. L., "Active Warping Control of a Joined Wing Airplane Configuration," AIAA/ASME/ASCE/AHS/ASC Structures, Structural Dynamics, and Materials Conference, Hampton, VA, 2003.

21. Cesnik, C. E. S. and Ortega-Morales, M., "Active Aeroelastic Tailoring of Slender Flexible Wings," International Forum on Aeroelasticity and Structural Dynamics, Madrid, Spain, 2001.

22. Blair, M. and Canfield, R., "A Joined-Wing Structural Weight Modeling Study," AIAA/ASME/ASCE/AHS/ASC Structures, Structural Dynamics, and Materials Conference, Denver, CO, Apr 2002.

23. Danielson, D. A. and Hodges, D. H., "Nonlinear Beam Kinematics by Decomposition of the Rotation Tensor," *Journal of Applied Mechanics*, Vol. 54, 1987, pp. 258–262.

24. Danielson, D. A. and Hodges, D. H., "A Beam Theory for Large Global Rotation, Moderate Local Rotation, and Small Strain," *Journal of Applied Mechanics*, Vol. 55, 1988, pp. 179–184.

25. Parker, D. F., "The Role of Saint Venant's Solutions in Rod and Beam Theories," *Journal of Applied Mechanics*, Vol. 46, 1979, pp. 861–866.

26. Atilgan, A. R. and Hodges, D. H., "A geometrically nonlinear analysis for nonhomogeneous, anisotropic beams," Proc. 30th AIAA/ASME/ASCE/AHS/ASC Structures, Structural Dynamics, and Materials Conference, Mobile, AL, 3-5 April 1989.

27. Reissner, E., "On one-dimensional large-displacement finite-strain beam theory," *Studies in Applied Mathematics*, Vol. 52, 1973, pp. 87–95.

28. Reissner, E., "On finite deformations of space-curved beams," *ZAMP*, Vol. 32, 1981, pp. 734–744.

29. Borri, M. and Mantegazza, P., "Some Contributions on Structural and Dynamic Modeling of Helicopter Rotor Blades," *l'Aerotecnica Missili e Spazio*, Vol. 64, 1985, pp. 143–154.

30. Bachau, O. and Kang, N., "A Multibody Formulation for Helicopter Structural Dynamic Analysis," *Journal of the American Helicopter Society*, Vol. 38, 1993, pp. 3–14.

31. Berdichevskii, V. L., "Equations of the theory of anisotropic inhomogeneous rods," *Dokl. Akad. Nauk. SSR*, Vol. 228, 1976, pp. 558–561.

32. Popescu, B. and Hodges, D. H., "On asymptotically correct Timoshenko-like anisotropic beam theory," *International Journal of Solids and Structures*, Vol. 37, 2000, pp. 535–558.

33. Yu, W., Volvoi, D., Hodges, D. H., and Hong, X., "Validation of the Variational Asymptotic Beam Sectional (VABS) Analysis," *AIAA Journal*, Vol. 40, 2002, pp. 2105–2112.

34. Yu, W., Volovoi, V. V., Hodges, D. H., and Hong, X., *Manual of VABS*, 2008.

35. *MD Nastran R3 Release Guide*, 2008.

36. Kuhn, P., *Stress in Aircraft and Shell Structures*, McGraw-Hill Book Company, Inc., New York, NY, 1956.

REPORT DOCUMENTATION PAGE

Form Approved
OMB No. 0704–0188

The public reporting burden for this collection of information is estimated to average 1 hour per response, including the time for reviewing instructions, searching existing data sources, gathering and maintaining the data needed, and completing and reviewing the collection of information. Send comments regarding this burden estimate or any other aspect of this collection of information, including suggestions for reducing this burden to Department of Defense, Washington Headquarters Services, Directorate for Information Operations and Reports (0704–0188), 1215 Jefferson Davis Highway, Suite 1204, Arlington, VA 22202–4302. Respondents should be aware that notwithstanding any other provision of law, no person shall be subject to any penalty for failing to comply with a collection of information if it does not display a currently valid OMB control number. PLEASE DO NOT RETURN YOUR FORM TO THE ABOVE ADDRESS.

1. REPORT DATE (DD–MM–YYYY)	2. REPORT TYPE	3. DATES COVERED *(From — To)*
18-06-2009	Master's Thesis	Jan 2008 – Jun 2009

4. TITLE AND SUBTITLE
Structural Optimization of Joined-Wing Beam Model with Bend-Twist Coupling Using Equivalent Static Loads

5a. CONTRACT NUMBER

5b. GRANT NUMBER

5c. PROGRAM ELEMENT NUMBER

6. AUTHOR(S)
Green, Nicholas S., LCDR, USN

5d. PROJECT NUMBER

5e. TASK NUMBER

5f. WORK UNIT NUMBER

7. PERFORMING ORGANIZATION NAME(S) AND ADDRESS(ES)
Air Force Institute of Technology
Graduate School of Engineering and Management (AFIT/ENY)
2950 Hobson Way
WPAFB OH 45433-7765

8. PERFORMING ORGANIZATION REPORT NUMBER
AFIT/GAE/ENY/09-J01

9. SPONSORING / MONITORING AGENCY NAME(S) AND ADDRESS(ES)
Air Force Research Laboratory Air Vehicles Directorate
Attn: Dr. Maxwell Blair
210 8th St Bldg 146
Wright-Patterson Air Force Base, OH 45433

10. SPONSOR/MONITOR'S ACRONYM(S)
AFRL/RBSD

11. SPONSOR/MONITOR'S REPORT NUMBER(S)

12. DISTRIBUTION / AVAILABILITY STATEMENT
APPROVED FOR PUBLIC RELEASE; DISTRIBUTION UNLIMITED

13. SUPPLEMENTARY NOTES
This material is declared a work of the U.S. Government and is not subject to copyright protection in the United States.

14. ABSTRACT
This study is based on the merger of two separate theories to further the efficiency with which joined-wing structural models are designed. The first theory is Geometrically Exact Beam Theory (GEBT). GEBT is a small strain beam theory which is capable of accurately capturing the geometric bend-twist coupling in beam elements that are experiencing large global deformations. This is crucial to the joined-wing problem as it is geometrically nonlinear. The second theory concerns Equivalent Static Loads (ESL). These ESL consist of a load vector that produces the same nodal displacements and rotations as those computed from a pure nonlinear analysis. The ESL displacements and rotations are then used to calculate ESL stresses. By merging these two theories into a single structural optimization effort, computational cost is reduced by orders of magnitude when compared to purely nonlinear response optimization efforts. It is shown that the final design obtained by the optimization is the same for both types of analysis. The final result is a much simpler model than a detailed finite element model of the joined-wing aircraft that can be optimized without significant loss in fidelity in a fraction of the time required for a single nonlinear response optimization cycle using finite element analysis.

15. SUBJECT TERMS
Joined-Wing, GEBT, Equivalent Static Loads, Optimization

16. SECURITY CLASSIFICATION OF:			17. LIMITATION OF ABSTRACT	18. NUMBER OF PAGES	19a. NAME OF RESPONSIBLE PERSON
a. REPORT	b. ABSTRACT	c. THIS PAGE			Swenson, Eric D., Lt Col, USAF (ENY)
U	U	U	UU	80	19b. TELEPHONE NUMBER (Include Area Code) (937)785-3636 x7479 e-mail: Eric.Swenson@afit.edu